UNIVERSIDAD DE CHILE
FACULTAD DE CIENCIAS FÍSICAS Y MATEMÁTICAS
DEPARTAMENTO DE INGENIERÍA CIVIL

IMPLICANCIAS DEL USO DE BANDAS DE ELEVACIÓN EN UN MODELO HIDROLÓGICO A MACRO-ESCALA: APLICACIÓN EN CUENCAS ANDINAS DE CHILE CENTRAL

TESIS PARA OPTAR AL GRADO DE MAGÍSTER EN CIENCIAS DE LA INGENIERÍA, MENCIÓN RECURSOS Y MEDIO AMBIENTE HÍDRICO

MEMORIA PARA OPTAR AL TÍTULO DE INGENIERO CIVIL

OCTAVIO ALFONSO MURILLO QUIJADA

PROFESOR GUÍA:

PABLO MENDOZA ZÚÑIGA

MIEMBROS DE LA COMISIÓN:

XIMENA VARGAS MESA

ÁLVARO AYALA RAMOS

SANTIAGO DE CHILE

2022

RESUMEN DE LA TESIS PARA OPTAR AL GRADO DE: Magíster en Ciencias de la Ingeniería, mención Recursos y Medio Ambiente Hídrico
RESUMEN DE LA TESIS PARA OPTAR AL TÍTULO DE: Ingeniero Civil
POR: Octavio Alfonso Murillo Quijada
FECHA: 2022
PROFESOR GUIA: Pablo Mendoza Zúñiga

IMPLICANCIAS DEL USO DE BANDAS DE ELEVACIÓN EN UN MODELO HIDROLÓGICO A MACRO-ESCALA: APLICACIÓN EN CUENCAS ANDINAS DE CHILE CENTRAL

La implementación de bandas de elevación es una estrategia común para incorporar gradientes verticales en temperatura, precipitación, y/u otras variables meteorológicas que inciden en la acumulación y derretimiento de nieve en zonas de topografía compleja. Sin embargo, la configuración de bandas usualmente se basa en la experiencia del/la modelador/a o investigaciones similares, sin existir – hasta la fecha – un estudio que documente en forma sistemática las implicancias hidrológicas de esta decisión y que ofrezca lineamientos sobre qué sub-dominios son más sensibles a ella. Por lo tanto, este trabajo de tesis busca llenar esta brecha, para lo cual se configura el modelo hidrológico distribuido de macro-escala VIC en nueve cuencas ubicadas en los Andes chilenos extratropicales, comparándose los resultados de simulaciones que no consideran bandas de elevación con simulaciones provenientes de configuraciones alternativas, que consideran discretizaciones verticales cada 1000, 750, 500, 200 y 100 m al interior de cada celda. Específicamente, se analizan las variaciones que introducen dichas configuraciones en la calidad de las simulaciones de caudal medio diario y mensual, el balance hídrico anual – tanto a la escala de cuenca como de celda –, y simulaciones de equivalente en agua de nieve (EAN). En todos los experimentos, se consideran sólo variaciones verticales de temperatura dentro de cada celda, y los análisis se efectúan en un período climatológico (Abril/1982 – Marzo/2015), un periodo húmedo (Abril/1982 – Marzo/1987) y un periodo seco (Abril/2010 – Marzo/2015).

Los resultados muestran que añadir bandas de elevación afecta principalmente la partición de precipitación que cae en forma líquida y sólida, y el equivalente de agua de nieve (EAN) del 1 de septiembre, tanto a las escalas de cuenca como de celda. Sin embargo, los efectos en el caudal modelado son poco apreciables, lo que sugiere que existe equifinalidad proveniente de estructuras de modelo. Además, se obtiene que los flujos se ven más afectados por la inclusión de bandas durante los años húmedos, mientras que el EAN del 1 de septiembre cambia más durante los años secos. En general, el efecto de añadir bandas de elevación se ve progresivamente reducido mientras mayor discretización vertical se considere, y puede variar entre las cuencas; además, el aumento de la discretización vertical tiene un efecto no lineal sobre los flujos y variables de estado. Finalmente, se identifican las celdas en las que el EAN del 1 de septiembre se ve más afectado por la inclusión de bandas de elevación, por lo que se recomienda que, en trabajos futuros, al menos las celdas con menor altitud media, cuyo rango de elevación sea mayor a 1000 m y que posean una pendiente pronunciada (mayor a 15°), sean modelados con bandas de elevación.

AGRADECIMIENTOS

En primer lugar, quiero agradecer a mi familia, por todo el apoyo que me han dado y el crecimiento que hemos logrado en conjunto. Espero que nos sigamos apoyando en nuestros proyectos.

A mis amigos del colegio, Naty y Laury, por todos estos años que llevamos de amistad y las interminables juntas. Verlos crecer ha sido un privilegio.

También a mis amigas de la época del preuniversitario, Bawi y Catalí. Bawi, admiro la resilencia después de tu problema de salud. Catalí, has sido, eres y serás lo máximo.

A todos los amigos y compañeros, partiendo por la Sección 3 y los amigos del Pasillo (Gabo, Cami, Tomy, Cris, Lecaros, Carly, Diomedi, Marcelo, Talo, Vale y tantos otros). Las salidas a la playa y los cumpleaños fueron las mejores y son lo máximo como personas. A amigos que conocí y compartí en el camino, a quienes les deseo lo mejor (Dani L., Dani G., Cárcamo). Mención honrosa a los Panesaurios Isis, Martín, Hugo y Joaquín, por la compañía, especialmente en los últimos años. Siempre es un placer hablar, jugar y compartir. Y segunda mención honrosa a la Cami Zúñiga, que se lo merece.

Agradezco a todos quienes me brindaron su amistad en el Civil, especialmente a Los Arrieros (Lulo, Diego, Michi, Fran, Basti, Cyntia, Ariel, Claudio, Cata, Karina). Estuvieron siempre presente en las eternas tardes de estudio y tareas. La salita de estudio del departamento debería rebautizarse.

A quienes conocí en la especialidad del departamento, Cote, Pipe, Cata, Javi Lecourt, Isa, Joseph. Hicieron el paso por la universidad mucho más agradable.

Entregar mi gratitud a mis compañeros del magíster, en especial con quienes fui más cercano (Micol, Catalina, Nery). Mención honrosa a la Micol, por todo lo compartido, trabajado y conversado. Agradecer también el apoyo de Nicolás Vásquez en todo este proceso.

Quiero entregar mi gratitud a todos los docentes del tercer piso del Departamento de Ingeniería Civil, en particular a aquellos que me permitieron ser parte de sus Equipos Docentes. En especial a la profesora Ana Lucía Prieto, con quien compartí mi primera experiencia como ayudante y como auxiliar. Sin duda alguna, de las mejores decisiones que he tomado en la universidad.

Agradecer a Jacqueline Suárez por su disposición y apoyo. Y a los profesores Yarko Niño, Aldo Tamburrino y Ximena Vargas, quienes llevan el programa del magíster a sus espaldas.

Mencionar a mi comisión de tesis, quien me brindó valiosos apoyos para mejorar la investigación.

A la selección de Judo de la Universidad de Chile, con quienes hemos compartido experiencia, sudor y lágrimas en estos años de universidad. Son un equipo excepcional.

Agradezco especialmente a mi profesor guía Pablo Mendoza, por todo el apoyo que me ha brindado durante estos años, desde ser parte del Equipo Docente de Hidrología, la docencia, el ingreso al magíster y el desarrollo de este proyecto. Sin duda alguna, de las mejores personas del departamento. Gracias por estar siempre atento, siempre motivado y traspasar la pasión por la investigación.

Esta tesis fue parcialmente apoyada por la infraestructura de supercómputo del NLHPC (ECM-02).

TABLA DE CONTENIDO

I. INTRODUCCIÓN

El desarrollo del manto nival es esencial para la disponibilidad de agua en ambientes montañosos. En este contexto, los modelos numéricos son útiles para el entendimiento de los procesos físicos que determinan la acumulación y el derretimiento de la nieve (e.g., Liston & Sturm, 1998; Lehning et al., 2006; Clark et al., 2017), así como para realizar predicciones hidrológicas que puedan ser usadas por tomadores de decisión y autoridades (Schneider & Molotch, 2016), considerando cambios proyectados en las condiciones climáticas (IPCC, 2021). Se espera que dichos cambios afecten al manto de nieve en diversas regiones montañosas del mundo (Barnett et al., 2005), entre las que se encuentran las cuencas de cabecera del río Colorado, Estados Unidos (e.g., Rasmussen et al., 2014), las montañas Apalaches, Estados Unidos (Demaria et al., 2016), los Himalayas de Nepal (Bhatta et al., 2019), los Andes extratropicales (Vicuña et al., 2021) y los Pirineos españoles (López-Moreno et al., 2013). Por lo tanto, mejorar la representación de los procesos nivales en modelos hidrológicos es esencial para estimaciones más confiables de equivalente en agua de nieve (EAN) en condiciones climáticas presentes y futuras.

En el caso particular de los Andes extratropicales, es de vital importancia comprender y caracterizar la heterogeneidad espacial de la nieve, dada su importancia en la hidrología de Chile y Argentina y, por lo tanto para los ecosistemas y las comunidades humanas que se desarrollan a lo largo y ancho de este dominio (Masiokas et al., 2020; Mendoza et al., 2020). Estudios previos en la cordillera de los Andes han recurrido a modelos numéricos para realizar proyecciones de cambio climático (Vargas et al., 2013; Aguayo et al., 2021), para entender la conceptualización y la estructura que debe tener un modelo para modelar los procesos físicos dominantes (Ragettli et al., 2014) o para documentar la sensibilidad relativa de modelos a la parametrización y a las forzantes meteorológicas (Voordendag et al., 2021).

Debido a que los estudios de disponibilidad hídrica en áreas montañosas se realizan típicamente a la escala de cuenca o a escala regional (Mendoza et al., 2020), se requieren estrategias de discretización espacial para representar heterogeneidades espaciales dentro del dominio de interés. Para ello, es común el delineamiento de grillas (e.g., Liang et al., 1996; Beck et al., 2020), subcuencas (e.g., Bandaragoda et al., 2004) y Unidades de Respuesta Hidrológica (URH; Markstrom et al., 2008; Newman et al., 2014). Además, es común incorporar estrategias para representar la distribución espacial del EAN dentro de cada unidad de modelación (Hartman et al., 1999; Pradhanang et al., 2011; Bajracharya et al., 2018) y para reducir la sensibilidad del modelo a cambios en su escala espacial (Haddeland et al., 2002). Un enfoque típico para representar variaciones verticales en modelos de *land-surface* es la incorporación de bandas de elevación, las que pueden ser usadas para incluir los efectos orográficos en la precipitación y la temperatura (Abdulla et al., 1996), mejorar la simulación de la temporalidad del derretimiento de nieve (e.g., Habets et al., 1999; Vicuña et al., 2011) y las dinámicas de la escorrentía (Abbaspour et al., 2007).

A pesar del amplio uso que la comunidad hidrológica da a las bandas de elevación para la configuración de modelos, no existe un consenso sobre cuál es la configuración más apropiada, ni sus efectos en las variables hidrológicas simuladas (Grusson et al., 2015).

Estudios previos que han implementado bandas de elevación sólo proveen información del número de bandas (e.g., Abdulla et al., 1996; Andreadis & Lettenmaier, 2006; Li et al., 2017; Newman et al., 2017; Bajracharya et al., 2018) o de la discretización vertical (e.g., Fontaine et al., 2002; Haddeland et al., 2002; Arora et al., 2008), sin dar mayores detalles y/o justificación de su elección. Por lo tanto, mejorar la comprensión de cómo las bandas de elevación afectan los flujos y variables de estado simulados es crucial para una mejor caracterización de los recursos hídricos en zonas montañosas, considerando los grandes efectos detrás de decisiones subjetivas de modelación (Mendoza et al., 2016; Mizukami et al., 2016; Melsen et al., 2019).

Hasta la fecha, pocos estudios han examinado el efecto de configuración de bandas de elevación en aplicaciones con modelos hidrológicos. Arola y Lettenmaier (1996) encontraron que añadir 10 bandas de elevación a un modelo concentrado reduce las diferencias en el EAN simulado con respecto a un modelo distribuido agregado, en base a análisis efectuados en dos regiones en Montana. Hartman et al. (1999) configuraron el modelo RHESSys en la cuenca de Loch Vale, perteneciente al Parque Nacional de las montañas Rocosas (Colorado, Estados Unidos), y compararon el efecto de añadir bandas de elevación configuradas cada 200 m y cada 500 m con un modelo sin bandas de elevación. En su implementación, distribuyeron verticalmente la precipitación, la temperatura del aire y los flujos radiativos, encontrando pequeñas diferencias entre las configuraciones de modelos al simular el EAN a escala de cuenca, y concluyeron que añadir bandas de elevación afecta la temporalidad de la escorrentía simulada. Haddeland et al. (2002) compararon simulaciones generadas con bandas de elevación cada 200 m y sin bandas de elevación, utilizando el modelo *Variable Infiltration Capacity* (VIC; Liang et al., 1994) a diferentes resoluciones horizontales en las cuencas de los ríos Columbia y Arkansas; el no incorporar bandas de elevación provocó que el derretimiento ocurriese antes, se incrementara la evapotranspiración y, por lo tanto, cambiaran tanto en la temporalidad como en el volumen de escorrentía. Essery (2003) comparó el EAN promedio simulado de nueve inviernos en la cuenca del río Torne-Kalix en Escandinavia, obtenido desde un modelo espacialmente agregado, un modelo distribuido con diez bandas de elevación y un modelo totalmente distribuido a una escala de 0,25°; encontraron mayor coincidencia entre el modelo distribuido con bandas de elevación y aquel totalmente distribuido, los que produjeron un menor EAN máximo y una mayor duración de la cobertura de nieve (comparado al caso sin bandas de elevación), y encontraron mejoras mínimas en los resultados al ocupar entre cuatro y 10 bandas de elevación. Pradhanang et al. (2011) implementaron el modelo SWAT con ninguna, tres y cinco bandas de elevación (definidas con igual área) en la cuenca Cannonsville (Nueva York, Estados Unidos), distribuyendo diariamente la precipitación y la temperatura en función de la altitud con una regresión lineal simple. Concluyeron que las simulaciones de caudal mejoran al implementar tres bandas de elevación, con leves mejoras al incrementar ese número.

Recientemente, Grusson et al. (2015) mostraron en la cuenca Garonne, Francia, que implementar diez bandas de elevación en el modelo SWAT produce mejores simulaciones de caudal, mayor escorrentía y menos evapotranspiración que las dos simulaciones de referencia (que no consideraron bandas de elevación). Bhatta et al. (2019) caracterizaron los efectos de las decisiones geoespaciales al discretizar la cuenca del río Tamor (en los

Himalayas este, Nepal); en particular, encontraron que el paso entre una y cinco bandas de elevación produce una considerable mejora en las simulaciones de escorrentía diaria, mientras que incorporar entre cinco y diez bandas de elevación conlleva beneficios marginales. Ninguno de estos estudios evaluó sistemáticamente los efectos que la discretización vertical produce en las simulaciones de caudal y en los componentes del balance hídrico anual, o identificaron aquellas subregiones donde implementar las bandas de elevación conlleva grandes variaciones en el EAN simulado. Por lo tanto, este trabajo de tesis considera las siguientes preguntas de investigación:

1. ¿Cómo afecta la configuración de bandas de elevación a la simulación del caudal, de los flujos del balance hídrico anual a escala de cuenca y del EAN cercano a la fecha de máxima acumulación?
2. ¿Cuáles son las implicancias de añadir bandas de elevación al EAN simulado a escala de celda?
3. ¿Qué atributos caracterizan aquellas celdas en las cuales las bandas de elevación producen una mayor diferencia en el EAN simulado?

Para responder las preguntas planteadas, se configura el modelo hidrológico de macro-escala VIC en su modo de balance de energía en nueve cuencas ubicadas en los Andes chilenos extratropicales. Se comparan los resultados de simulaciones sin bandas de elevación con simulaciones que consideran discretizaciones verticales (bandas de elevación) sub-celda definidas cada 1000, 750, 500, 200 y 100 m. Se utiliza el modelo VIC dado (i) el interés global de usuarios (Addor & Melsen, 2019) y, por lo tanto, la potencial utilidad de los resultados de esta investigación para la comunidad hidrológica internacional y (ii) esfuerzos pasados y presentes para caracterizar la actual y futura hidrología a lo largo de Chile continental (DGA, 2017; Vásquez et al., 2021; Vicuña et al., 2021). Para eliminar el posible rol de las condiciones climáticas en las diferencias en el modelo, y en parte con la motivación de los efectos negativos en la presente mega sequía en Chile Central (Garreaud et al., 2017, 2019), se analizan diferencias entre configuraciones de modelos en un período climatológico (Abril/1982 – Marzo/2015), en un periodo húmedo (Abril/1982 – Marzo/1987) y en un periodo seco (Abril/2010 – Marzo/2015). Una diferencia clave con trabajos previos es que la investigación se enfoca en el efecto exclusivo de distribuir la temperatura del aire con la topografía, manteniendo las tasas de precipitaciones y el resto de las variables meteorológicas que influyen en el balance de energía de la cobertura nival espacialmente constantes a lo largo de cada celda. Sin embargo, ya que VIC calcula varios de los flujos de energía como función de la temperatura, se espera que estos flujos también tengan una variación vertical.

1.1. Objetivos

Los objetivos del presente trabajo son los siguientes:

1.1.1. Objetivos Generales

Evaluar el efecto que tiene la configuración de bandas de elevación en la caracterización hidrológica de cuencas con alguna componente nival.

1.1.2. Objetivos Específicos

- Analizar las implicancias que tiene la configuración espacial del módulo de nieves de VIC en (1) el Balance hídrico anual y (2) el balance hidrológico estacional a las escalas de pixel y de cuenca.
- Analizar los efectos dentro de distintos periodos hidroclimáticos.

II. ARTÍCULO PARA PUBLICACIÓN

A continuación, se presenta el artículo titulado "*Exploring the impacts of subgrid elevation bands on hydrological portrayals with a process-based model*":

Exploring the impacts of subgrid elevation bands on hydrological portrayals with a process-based model

Octavio Murillo[1], Pablo A. Mendoza[1,2], Nicolás Vásquez[1], and Naoki Mizukami[3]
[1]Department of Civil Engineering, Universidad de Chile, Santiago, Chile.
[2]Advanced Mining Technology Center (AMTC), Universidad de Chile, Santiago, Chile.
[3]National Center for Atmospheric Research (NCAR), Boulder, Colorado, USA.

Abstract

The implementation of elevation bands is a common strategy to include vertical heterogeneity in hydrology and land surface models, and therefore improve simulations of snow water equivalent (SWE). However, there is not consensus in the community about recommended guidelines for their delineation, which is typically based on subjective reasons. In this paper, we characterize hydrological implications of this choice by configuring the Variable Infiltration Capacity (VIC) model in nine basins located in the western slopes of the Andes Cordillera, central Chile, using six different configurations: no elevation bands (benchmark model), and elevation bands with a vertical discretization of 1000, 750, 500, 200 and 100 m. The analyses are conducted in a wet period (April/1982-March/1987), dry period (April/2010-March/2015) and a climatological period April/1982-March/2015). The results show that adding elevation bands does not yield considerable variations in simulated monthly or daily streamflow; however, there are important effects on the partitioning of precipitation between snowfall and rainfall, snowmelt, sublimation, and the spatial variability in September 1 SWE, suggesting a model-structure equifinality. Incorporating elevation bands generally yields less basin-averaged snowmelt, and more (less) catchment-scale sublimation across water-limited (energy-limited) basins. We also found that the implications of subgrid elevation bands vary with the analysis period: fluxes are more affected during the wet period, while variations in September 1 SWE are more noticeable during the dry period. In general, the effects of adding elevation bands are reduced with increasing vertical discretization, and can differ among catchments. Finally, our results indicate that the grid cells that yield the largest sensitivities in the configuration of elevation bands have relatively lower mean altitude, elevation ranges >1000 m, steep slopes (>15°) and annual precipitation amounts <1000 mm that concentrate within a few months.

1. Introduction

Snow is essential for water supply in mountain environments. In this context, numerical models are not only useful for understanding the physical processes that determine snow accumulation and melting (Liston & Sturm, 1998; Lehning et al., 2006; Clark et al., 2017), but also to make predictions that can be used for decision making (Schneider & Molotch, 2016), especially considering ongoing and future changes in climatic conditions (IPCC, 2021). Indeed, climate change is expected to impact mountain snowpack in many mountain regions of the world (Barnett et al., 2005), such as the Colorado Headwaters of USA

(Rasmussen et al., 2014), the Appalachian Mountains (Demaria et al., 2016), the eastern Himalayas of Nepal (Bhatta et al., 2019), the extratropical Andes (Vicuña et al., 2021), and the Spanish Pyrenees (López-Moreno et al., 2013). Hence, improving the realism of snow models is critical for reliable estimates of snow water equivalent (SWE) under current and future climatic conditions.

Because water resources applications in mountainous areas require model simulations at the watershed or regional scales (Mendoza et al., 2020), spatial discretization strategies are needed to address heterogeneities within the domain of interest. Common choices involve the delineation of grid cells (Liang et al., 1996; Beck et al., 2020), sub-catchments (Bandaragoda et al., 2004) and hydrologic response units (Markstrom et al., 2008; Newman et al., 2014) as a spatial modeling unit. Typically, sub-element variability is also incorporated to improve simulation of the spatial distribution of SWE within each modeling unit (Hartman et al., 1999; Pradhanang et al., 2011; Bajracharya et al., 2018) and to reduce the model sensitivity to changes in the spatial scale (Haddeland et al., 2002). A popular approach is the implementation of subgrid elevation bands, which can account for orographic effects on precipitation and temperature (Abdulla et al., 1996), improving the timing of simulated snowmelt (e.g., Habets et al., 1999; Vicuña et al., 2011) and streamflow dynamics (Abbaspour et al., 2007).

Despite the widespread use of elevation bands in the hydrology modeling, there is no guidance for appropriate configuration, based on the effects on simulated hydrological variables (Grusson et al., 2015). Indeed, many studies implementing elevation bands only provide information on the number of snow bands (e.g., Abdulla et al., 1996; Andreadis & Lettenmaier, 2006; Li et al., 2017; Newman et al., 2017; Bajracharya et al., 2018) or the vertical discretization (e.g., Fontaine et al., 2002; Haddeland et al., 2002; Arora et al., 2008), without further details and/or justification of their choice. Improved understanding of effects of elevation bands on simulated states and fluxes is crucial for better characterization of water resources in mountain domains, given the large effects that subjective modeling decisions may have on hydrological portrayals (Mendoza et al., 2016; Mizukami et al., 2016; Melsen et al., 2019).

To the best of our knowledge, only a few studies have examined the effects of elevation band configurations on hydrologic model simulations. Arola and Lettenmaier (1996) found that adding 10 elevation bands to a lumped model configuration reduced differences in simulated SWE with respect to spatially-aggregated distributed model output in two regions in Montana, USA. Hartman et al. (1999) configured the RHESSys model in the Loch Vale Watershed (Rocky Mountains National Park, Colorado, USA) and compared the effects of adding 200-m and 500-m elevation bands against no bands. In their implementation, they distributed precipitation, air temperature and radiation fluxes at each band, finding (1) little differences among model configurations in catchment-averaged simulated SWE and annual runoff, and (2) that adding elevation bands affected the timing of simulated streamflow. Haddeland et al. (2002) compared model simulations between a 200-m elevation band configuration and no elevation bands, running the Variable Infiltration Capacity (VIC; Liang et al., 1994) model across different grid resolutions over the Columbia and Arkansas River

basins; when no elevation bands were considered, melting occurred earlier, with an increase in evapotranspiration (ET) and, therefore, a shift in both timing and amount of runoff. Essery (2003) compared domain-averaged SWE simulations for the Torne-Kalix River basin (Scandinavia), obtained from a spatially aggregated model, a distributed model with 10 elevation bands, and a 0.25° fully distributed model; they found a close agreement between the latter two configurations, which produced lower peak SWE and a longer snow cover duration (compared to the case without bands), and found little improvements using four to 10 elevation bands. Clark et al. (2011) showed that disaggregating the Pinnacle Stream subcatchment (New Zealand) into 100-m elevation bands produced much lower basin-averaged melt rates compared to a spatially lumped configuration. Pradhanang et al. (2011) implemented and calibrated the SWAT model with none, three and five elevation bands (defined with equal areas) in the Cannonsville watershed (New York, USA), distributing daily precipitation and temperature using a simple linear regression with altitude; they found that streamflow simulations were improved when using three elevation bands, with little impacts when further increasing the number of elevation bands.

More recently, Grusson et al. (2015) showed that implementing ten elevation bands in the SWAT model yielded better streamflow simulations, more runoff and less evapotranspiration than two reference simulations (without bands) in the Garonne watershed in France. Bhatta et al. (2019) characterized the effects of geospatial decisions when discretizing the Tamor River basin (eastern Himalayas, Nepal); in particular, they found that moving from one to five elevation bands provided considerable improvements in daily streamflow simulations, and that moving to 10 elevation bands yielded marginal benefits.

None of these studies systematically assessed the effects that the vertical discretization of elevation bands yields on streamflow simulations and annual water balance components, or identified those sub-regions where implementing elevation bands yields large variations in simulated SWE. Hence, this paper addresses the following research questions:

1. How does the configuration of elevation bands affect simulated streamflow, catchment-scale annual water balance and SWE near the date of maximum accumulation?
2. What are the implications of adding elevation bands on simulated SWE at the grid cell scale?
3. What attributes characterize those grid cells where elevation bands make a large difference in simulated SWE?

To seek for answers, we configure the VIC macro-scale hydrological model in nine basins located along the western slopes of the extratropical Chilean Andes. We compare simulation results from a calibrated model without elevation bands (benchmark) with those considering a vertical discretization defined every 1000, 750, 500, 200 and 100 m. We select the VIC model given: (i) the global interest of users (Addor & Melsen, 2019; Sepúlveda et al., 2021) and, therefore, the potential utility of our results for the hydrology community, and (ii) past and ongoing efforts to characterize the current and future hydrology across continental Chile (DGA, 2017; Vicuña et al., 2021; Vásquez et al., 2021). To disentangle the possible role of climatic conditions on inter-model differences, and partially motivated by the negative

effects of the ongoing megadrought in Central Chile (Garreaud et al., 2017, 2019), we conduct our assessments for a climatological period (April/1982 – March/2015), a wet period (April/1982 – March/1987) and a dry period (April/2010 – March/2015). A key difference with previous work is that we focus on the sole effects of distributing air temperature with topography, keeping precipitation rates and the rest of meteorological forcings spatially constant across every grid cell.

2. Study domain

We conduct our analyses in nine basins located along the western slopes of the extra-tropical Andes Cordillera (32.5°-37°S, 70°-71.5°W, Figure 1). These basins were selected based on the following criteria: (i) a near-natural flow regime defined as a maximum threshold value of 5% for the relationship between annual volume of water assigned as permanent consumptive rights and the mean annual flow (Table 3 in Alvarez-Garreton et al., 2018), (ii) absence of large reservoirs within each catchment, and (iii) small (<2%) glacierized area. Further, these catchments span a wide range of hydroclimatic conditions (Table 1), from high aridity index (2.9) and relatively low mean annual precipitation (486 mm; Estero Pocuro en el Sifón) to low aridity index (0.7) and high mean annual precipitation (1929 mm; Río Ñuble en La Punilla). The southern basins (35°-37°S in Figure 1) also have larger vegetation coverage (just forest fraction coverage shown) due to the lower aridity and increased precipitation, providing higher runoff ratios.

Additionally, our case study basins encompass different hydrological regimes (left and right panels in Figure 1), including rainfall-driven (Pocuro); snow-dominated (Las Leñas); and basins with mixed regimes where (i) rainfall is the main control for runoff production (Claro), (ii) rainfall and snowmelt contributions are comparable (Ñuble), or (iii) snowmelt dominates catchment-scale hydrology (Arrayán, Mapocho, Colorado, Los Palos and Melado). Interestingly, there are catchments where the seasonal cycles of soil moisture and runoff are very similar, regardless of their hydrological regimes (Claro, Las Leñas, Colorado, Palos and Melado), and basins where these cycles are very different (Arrayán, Mapocho, Claro and Ñuble).

Table 1. List of catchment attributes. Hydrologic variables correspond to the period April 1979 to March 2015. Mean slope and forest fraction were obtained from Alvarez-Garreton et al. (2018)

Catchment	Latitude (°)	Longitude (°)	Area (km^2)	Mean basin elevation and range (m.a.s.l)	Mean slope (°)	Mean Annual Precipitation (mm/yr)	Mean Annual AI (PET/P)	Mean Annual Runoff (mm/yr)	Mean Annual Runoff Ratio (-)	Forest fraction (%)
Estero Pocuro en el Sifón	-32.92	-70.54	181	2107 (1002-3695)	22.1	486	2.9	126	0.26	0.2
Estero Arrayán en la Montosa	-33.33	-70.46	216	2469 (969-3833)	24.2	615	2.4	233	0.38	0.4
Río Mapocho en Los Almendros	-33.37	-70.45	638	2936 (970-5428)	25.2	503	2.5	310	0.62	0.4
Río Las Leñas antes junta Río Cachapoal	-34.36	-70.31	172	2865 (1279-4574)	30.4	1266	1.1	752	0.59	0.2
Río Claro en El Valle	-34.69	-70.87	349	1596 (535-3334)	22.2	1422	0.9	862	0.61	27.1
Río Colorado en junta con Palos	-35.28	-71.00	877	2253 (594-4073)	19.6	1802	0.8	1387	0.77	11.5

Catchment	Latitude (°)	Longitude (°)	Area (km^2)	Mean basin elevation and range (m.a.s.l)	Mean slope (°)	Mean Annual Precipitation (mm/yr)	Mean Annual AI (PET/P)	Mean Annual Runoff (mm/yr)	Mean Annual Runoff Ratio (-)	Forest fraction (%)
Río Palos en junta con Colorado	-35.27	-71.02	490	2013 (595-4037)	19.9	1891	0.7	1689	0.89	16.7
Río Melado en el Salto	-35.88	-71.02	2127	2010 (698-3619)	23.5	1766	0.8	1232	0.70	1.9
Río Ñuble en La Punilla	-36.66	-71.32	1254	1711 (566-2617)	23.92	1929	0.7	1718	0.89	13.6

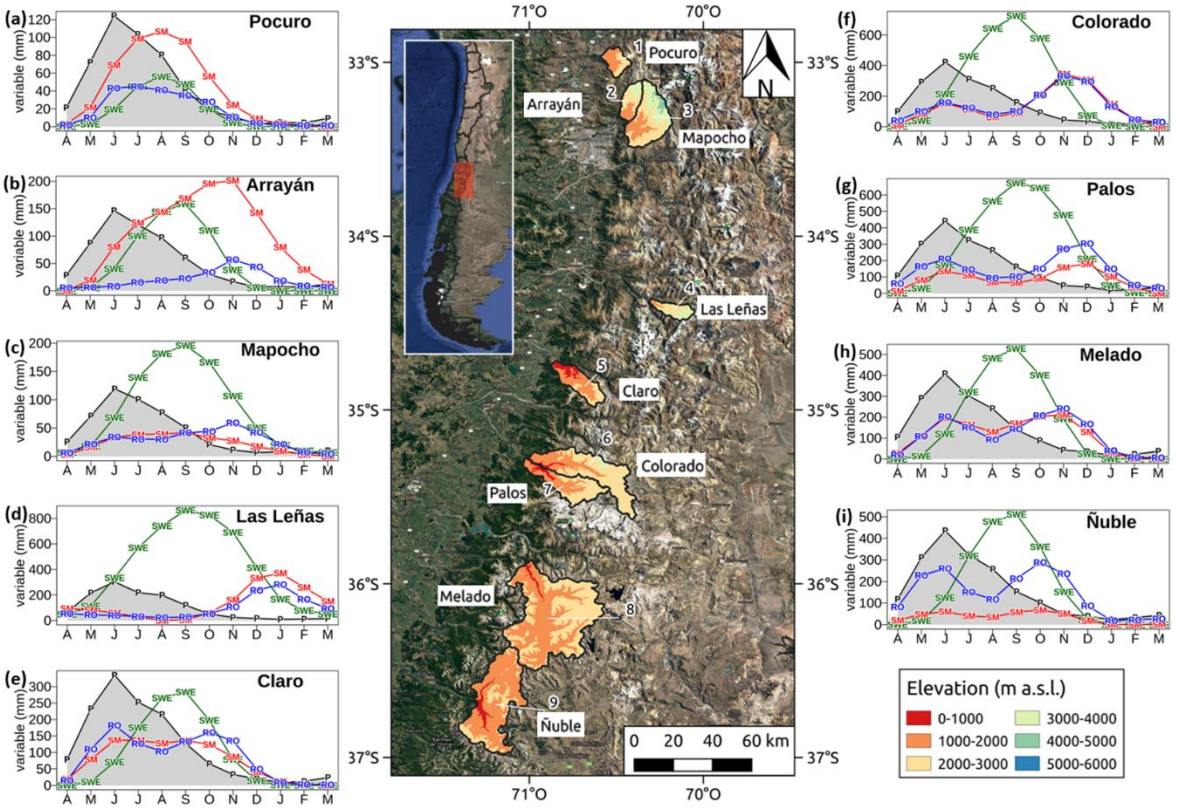

Figure 1. Location and elevation of the nine case study basins (center panel), along with seasonal cycles with precipitation (P, black lines and grey areas) and simulated water balance variables (left and right panels) for the climatological period (April/1982-March/2015) - including active soil moisture (SM, red), SWE (green) and runoff (RO, blue) - for the nine case study basins: (a) Estero Pocuro en el Sifón, (b) Estero Arrayán en la Montosa, (c) Río Mapocho en Los Almendros, (d) Río Las Leñas antes junta Río Cachapoal, (e) Río Claro en El Valle, (f) Río Colorado en junta con Palos, (g) Río Palos en junta con Colorado, (h) Río Melado en el Salto, (i) Río Ñuble en La Punilla. For modeled SM, we subtract the lowest mean monthly value of the year so that the plotted values show only the active range of variation.

3. Data and methods

3.1. Meteorological forcings and streamflow data

Daily precipitation and temperature extremes are obtained from an updated version of the CR2MET dataset (DGA, 2017), which has a horizontal resolution of 0.05° x 0.05°, covering Continental Chile for the 1979-2016 period. The dataset for precipitation was generated with a statistical postprocessing technique using topographic descriptors and large-scale climatic variables (water vapor and moisture fluxes) from ERA-Interim (Dee et al., 2011) and ERA5 (C3S & Copernicus Climate Change Service (C3S), 2017) as predictors, and observed daily precipitation from gauge stations as predictand. For the case of maximum and minimum daily temperature, additional variables from MODIS land surface products were added as predictors. Daily precipitation and temperature time series are disaggregated into 3-hourly time steps using the sub-daily distribution provided by ERA-Interim. Relative humidity and wind speed are derived for the same horizontal resolution grid by spatially interpolating a blend between ERA-Interim and ERA5 datasets. The blend between these products was created because ERA5 was not available for the entire study period (1985–2015) at the moment of data acquisition (early 2018). Despite the short temporal coverage from ERA5 (2010-2016), the updated reanalysis information was included for a better spatial representation of the mega drought (Garreaud et al., 2019; Vicuña et al., 2021).

Streamflow data is obtained from stations maintained by the Chilean Water Directorate (DGA, available from the CR2 Climate Explorer https://www.cr2.cl/datos-de-caudales/).

3.2. Hydrological model

We use the Variable Infiltration Capacity (VIC; Liang et al., 1994, 1996) model, which is a macro-scale, process-based and semi-distributed hydrologic model. In VIC, the modeling unit is the grid cell, which is defined here to match the meteorological forcing data resolution (i.e., 0.05° x 0.05°). The model is run at a 3-hourly time step. Interception is simulated with a one-layer canopy reservoir that is emptied by canopy evaporation, transpiration, or throughfall, which occurs when additional precipitation exceeds the storage capacity of the canopy. Different vegetation classes are allowed in each grid cell through a mosaic approach, where water and energy balance terms are computed independently for each coverage class (vegetation and bare soil). Each grid cell has three soil layers: the two upper layers represent the interaction between soil moisture and vegetation, while the bottom layer simulates baseflow processes. It should be noted that VIC does not consider lateral exchange of fluxes between grid cells, which implies that water can only enter a grid cell from the atmosphere. A two-layer energy balance model is used to simulate snowpack dynamics: the upper layer solves the energy balance between the atmosphere and the snowpack, and the bottom layer stores the excess snow mass from the upper layer (Cherkauer & Lettenmaier, 2003; Andreadis et al., 2009).

3.3. Experimental setup

3.3.1. Benchmark model

To assess the effects of including elevation bands on simulated states and fluxes, we compare different VIC implementations against a benchmark model based on the work by Vásquez et al. (2021). In such implementation, a priori distributions for vegetation parameters were obtained using the land cover classes described in Zhao et al. (2016); spatial information on hydraulic conductivity values was obtained from the Natural Resources Data Center (CIREN for its acronym in Spanish) and all grid cells were considered flat (i.e., no elevation bands are defined). In our setup, all model simulations are conducted in full energy balance mode – dismissing frozen soil processes –, and no horizontal runoff routing is performed since, for the contributing catchment areas examined here, routing effects are not expected to be important at the daily (or longer) time scale (Gericke & Smithers, 2014; Beck et al., 2020). Therefore, modeled streamflow is obtained from basin-averaged runoff.

The parameters for the benchmark model (Table 2) are calibrated using the Shuffled Complex Evolution global optimization algorithm (SCE; Duan et al., 1993). All soil parameters are considered spatially constant within each catchment (i.e., no parameter regularization was considered). The objective function is the Kling-Gupta Efficiency metric (Gupta et al., 2009):

$$KGE = 1 - \sqrt{(r-1)^2 + (\alpha-1)^2 + (\beta-1)^2} \quad (1)$$

where r is the Pearson correlation coefficient between simulated and observed runoff; α is the ratio of the standard deviation of simulated values to the standard deviation of observed values; and β is the ratio between the mean of the simulated values to the mean of observations.

The calibration process required streamflow data for at least four years within the period 1990-2010, and if the minimum record length is not satisfied, the periods 1985-1990 and 2010-2015 are considered. All model simulations are conducted for the period 1979-2015, using the first 3 years to initialize model states. If two or more parameter sets yield the same KGE values, we select the one that maximizes the Nash-Sutcliffe efficiency (NSE; Nash & Sutcliffe, 1970). The parameter sets found in this step are used for subsequent modeling experiments (section 3.3.2) - i.e., no parameter recalibration is performed.

Table 2. List of VIC parameters and limits considered for calibration.

Parameter	Description	Units	Calibration range	
			Min	Max
infilt	Variable infiltration curve parameter (b_{infilt})	-	0.001	0.162
D_s	Fraction of Ds_{max} where non-linear baseflow begins	-	0.312	0.806
Ds_{max}	Maximum velocity of baseflow	mm/day	83.2	183.2
W_s	Fraction of maximum soil moisture where non-linear baseflow occurs	-	0.108	0.900
C	Exponent used in baseflow curve	-	3.0	10.9
$depth_1$	Thickness of each soil moisture layer	m	0.014	2.169
$depth_2$		m	0.418	5.281

Parameter	Description	Units	Calibration range	
			Min	Max
$depth_3$		m	0.173	3.753
K_{sat}	Saturated hydraulic conductivity	mm/day	1499	2565
Newalb	Fresh snow albedo		0.725	0.950
$Alb_{acum\ a}$	Snow albedo curve parameter	-	0.725	0.950
$Alb_{thaw\ a}$	Snow albedo curve parameter	-	0.883	0..920
T_{rain}	Minimum temperature for rainfall occurrence	°C	-2.735	3.446
r_{snow}	Snow surface roughness	m	1.24E-5	0.022

3.3.2. Alternative model configurations

Figure 2 illustrates how elevation bands can be configured in VIC. It can be noted that the model lumps all areas within the same elevation range into one band. Additionally, fluxes and state variables for each band are weighted by area fraction to provide grid-cell averages.

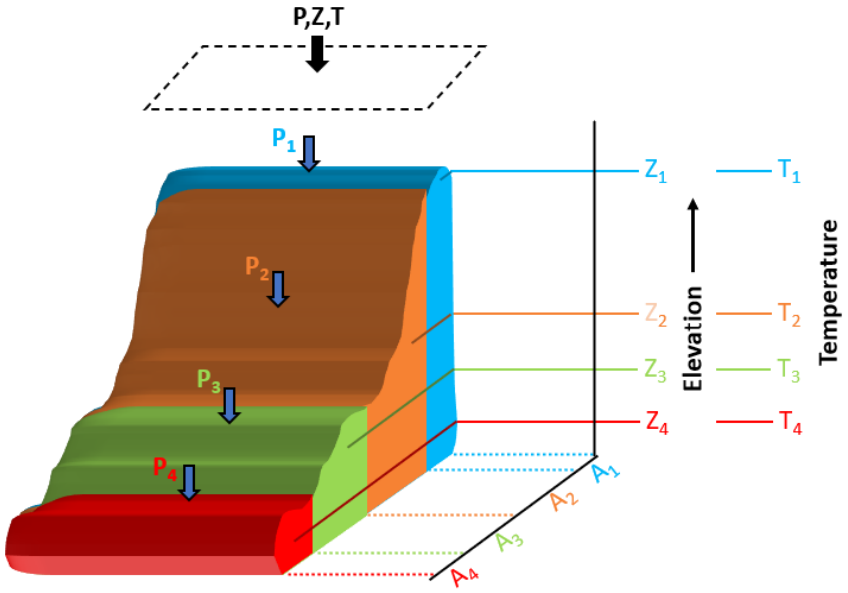

Figure 2. Spatial representation of subgrid elevation bands in VIC. A, P, T, and Z denote area, average precipitation, air temperature, and terrain elevation for each elevation band.

For each basin, we create five alternative model configurations by spatially disaggregating all grid cells into 1000 m, 750 m, 500 m, 200 m and 100 m elevation bands**,** using the Advanced Spaceborne Thermal Emission and Reflection (ASTER) global Digital Elevation Model. To harmonize all these spatial configurations, we consider 0 m a.s.l. as the starting point of elevation bands for all catchments, instead of the lowest point of each catchment's grid cell. For the lowest and the highest elevation bands, we set a minimum fractional area of 5% (with respect to the grid cell's area) to avoid creating redundant subunits; if such condition is not met, that band (i.e., the lowest and/or the highest) is merged to the closest

one. This implies that peak elevations may be excluded from our representation of subgrid variability.

In all alternative model configurations, precipitation rates are assumed to be constant with elevation, but air temperature is lapsed from the mean grid cell elevation to each elevation band using local lapse rates. To this end, we cluster our basins into three groups (basins 1-3, 4-7 and 8-9 in Figure 1) based on spatial proximity, and compute lapse rates using the mean annual temperatures obtained from the grid cells belonging to each cluster. It should be noted that these lapse rates are not affected by the configuration of elevation bands, since they are computed from a meteorological product (CR2MET) that assumes flat grid cells. All simulations with elevation bands are performed in full energy balance mode, without horizontal runoff routing.

3.3.3. Analysis framework

We select three continuous periods for analysis based on observed catchment-scale precipitation and runoff: (i) a 5-year wet period, (ii) a 5-year dry period, and (iii) a climatological period that spans April/1982 – March/2015, including (i) and (ii). The choice of wet and dry periods is based upon visual inspection of annual precipitation time series and the calculation of 5-year moving averages of precipitation and runoff. The wet period (April/1982 – March/1987) begins after a long epoch with a persistent negative trend in annual precipitation across the semi-arid central Chile (30-35°S) from the beginning of the 20th century until the mid-1970s (Quintana & Aceituno, 2012). Our dry period (April/2010 – March/2015) covers the first half of the megadrought, when severe annual rainfall deficits (25-45%) prevailed in central Chile (30-38°S), diminishing the Andean snowpack and resulting in amplified declines of river flow (up to 90%), reservoir volumes and groundwater levels (Garreaud et al., 2017).

First, we assess the capability of the benchmark model and each alternative model configuration (i.e., six model configurations in total) to reproduce observed daily runoff, flow duration curves and runoff seasonality. In this analysis, flow duration curves and runoff seasonality graphs are calculated for the climatological period. We compute the KGE and its components, and NSE for modeled runoff at daily and monthly time steps. Additionally, we examine the percent bias for the midsegment slope (%BiasFMS) and the low-segment volume (%BiasFLV) of the flow duration curves (Yilmaz et al. 2008):

$$\%\text{BiasFMS} = \frac{[log(QS_{m1}) - log(QS_{m2})] - [log(QO_{m1}) - log(QO_{m2})]}{[log(QO_{m1}) - log(QO_{m2})]} \cdot 100 \quad (2)$$

$$\%\text{BiasFLV} = -1 \cdot \frac{\sum_{l=1}^{L}[log(QS_l) - log(QS_L)] - \sum_{l=1}^{L}[log(QO_l) - log(QO_L)]}{\sum_{l=1}^{L}[log(QO_l) - log(QO_L)]} \cdot 100 \quad (3)$$

Then, we compute percent changes between alternative model configurations and the benchmark model results to quantify the effects of adding elevation bands on simulated input/output fluxes and SWE. Specifically, we examine mean annual rainfall, snowfall, runoff, sublimation, snowmelt and ET, as well as September 1 SWE (SWE 09/01 hereafter)

– which is used to produce operational seasonal streamflow forecasts in central Chile (Mendoza et al., 2014) –, at both catchment and grid cell (i.e., 0.05°) scales.

To analyze the effects of snow bands with different vertical discretizations on simulated daily SWE, we perform detailed analyses in three grid cells with different locations, mean elevations, and elevation ranges across the Mapocho River basin. These comparisons are conducted for water years selected from our wet and dry periods to disentangle the interplay between hydroclimatic conditions and the configuration of elevations bands. To identify the most sensitive grid cells and model configurations in terms of snow accumulation, we compare SWE 09/01 (i.e., SWE at the beginning of snowmelt season) obtained from the 200-m configuration and the benchmark, for all water years (i.e., 33) in the climatological period. We define a grid cell as sensitive if differences in simulated SWE 09/01 with respect to the benchmark model are larger than 10% for >50% of water years. To seek for controls on different grid cell behavior, we compare the cumulative distribution functions (CDFs) of several attributes (Table 3) obtained from sensitive vs. insensitive grid cells. We also contrast CDFs of state variables and fluxes simulated with the 200-m model configuration in sensitive vs. insensitive grid cells, including rainfall, snowfall, ET, runoff, snowmelt, and maximum SWE. In all these comparisons, we perform Kolmogorov-Smirnov tests and report associated p-values.

Table 3: Attributes considered for each grid cell. Calculations consider water years (April-March).

Attributes name	**Description**	**Units**	**Formula**
Altitude	Mean elevation	m a.s.l.	-
Range	Difference between maximum and minimum altitude.	m	$z_{max} - z_{min}$
Aspect	Average grid cell aspect, calculated counterclockwise from east.	°	-
Slope	Mean slope across each grid cell	°	-
Annual temperature (T)	Annual T for a specific water year	°C	$\frac{1}{N}\sum_{i=1}^{N} T_{daily}$
Annual precipitation (P)	Annual P for a specific water year	mm/yr	$\sum_{i=1}^{N} P_{daily}$
Annual Moisture Index (I_m)[1]	Indicates whether climatic conditions are arid (water-limited) or humid (energy-limited) .	-	$I_m = \frac{1}{12}\sum_{t=1}^{t=12} MI(t)$ Where:

[1] These climate indices were used in Knoben et al. (2018). It should be noted that the fraction of annual precipitation that occurs as snow (fs) was not calculated as in Knoben et al. (2018), because VIC computes snowfall considering a minimum temperature at which rainfall can occur and a maximum temperature at which snowfall can occur, rather than using a single temperature as threshold.

Attributes name	Description	Units	Formula
	Ranges from -1 to 1, with negative and positive values for arid and humid conditions, respectively.		$MI(t) = \begin{cases} 1 - \frac{E_P(t)}{P(t)} & , \quad P(t) > E_p(t) \\ 0 & , \quad P(t) = E_p(t) \\ \frac{P(t)}{E_P(t)} - 1 & , \quad P(t) < E_p(t) \end{cases}$
Moisture Index Seasonality (I_{mr})[1]	Indicates intra-annual changes in the water/energy budget. Ranges from 0 (no variability) to 2 (very large variability)	-	$I_{m,r} = \max\big(MI(1,2,\dots 12)\big) - \min\big(MI(1,2,\dots 12)\big)$
Fraction of annual precipitation that occurs as snow (f_s)[1]	Ranges from 0 to 1, where 0 indicates no snowfall in a year and 1 that all precipitation occurs as snow.	-	$f_s = \frac{\sum monthly\ snowfall}{\sum monthly\ precipitation}$

N is the number of days in each water year.

4. Results

4.1. Model evaluation against observed streamflow

Figure 3 compares modeled daily runoff time series against observations for water year (WY) 2009/2010 (as an example), as well as mean monthly runoff and daily flow duration curves for the climatological period. The results show small differences between the benchmark model (i.e., no elevation bands) and the alternative model configurations. Adding elevation bands provides a maximum KGE increment of 0.03 for daily streamflow throughout all basins during WY 2009/2010 (see Table 4). All model configurations underestimate daily peak flows during winter (e.g., f.1 and h.1) and fail to capture streamflow recessions, providing slower (e.g., see panel f.1 between June and August) or faster (e.g., see panel i.1 between July and August) responses compared to observed runoff. In the Palos River basin (Figure 3g.1), there are notable discrepancies in December arising from different vertical discretizations. Figure 3 also shows that all model configurations capture catchment-scale runoff seasonality reasonably well, excepting Estero Arrayán (panel b.2), where rainfall contributions to runoff are underestimated, or the Claro River basin, where modeled maximum monthly values are delayed. In some cases, observed monthly values are overestimated (e.g., Pocuro basin, panel a.2) or underestimated (e.g., December to March at the Ñuble basin, panel i.2; near August for g.2).

Table 4: KGE results of the daily runoff series - WY 2009/2010.

Model configuration	Pocuro	Arrayán	Mapocho	Las Leñas	Claro	Colorado	Palos	Melado	Ñuble
No Bands (NB)	0.73	0.58	0.58	0.79	0.51	0.64	0.70	0.69	0.32
1000 m	0.74	0.58	0.59	0.81	0.51	0.65	0.70	0.69	0.33

750 m	0.74	0.58	0.59	0.79	0.51	0.65	0.70	0.69	0.33
500 m	0.74	0.58	0.61	0.80	0.51	0.65	0.73	0.69	0.34
200 m	0.74	0.59	0.60	0.81	0.51	0.65	0.72	0.68	0.34
100 m	0.74	0.58	0.60	0.81	0.51	0.65	0.72	0.68	0.34

The results for the percent bias in the midsegment slope of the flow duration curves (%BiasFMS, Table 5) show that all model simulations yield flashier responses compared to observed runoff in all basins. When adding elevation bands, %BiasFMS increases in the Pocuro and Arrayán basins compared to the benchmark model, with maximum variations of 2.1% and 3.7% using the 100-m configuration, respectively, and these changes do not necessarily correlate with increased vertical resolution. However, elevation bands provide improvements (i.e., decrease in %BiasFMS) in the rest of the basins, ranging from 0.3% for the Claro River basin (200-m configuration) to 8.3% for Las Leñas River basin (200-m configuration).

The incorporation of elevation bands yields reductions in the percent bias in FDC low-segment volume (%BiasFLV, Table 5) in all catchments except the Mapocho River basin. As with %BiasFMS, improvements in %BiasFLV are not correlated with the vertical discretization, and they range from 0.01% for Pocuro (1000-m configuration) to 1.03% for Las Leñas (200-m configuration). However, large negative biases in simulated long-term baseflow responses are obtained in some basins (Figure 3, panels c.3, d.3, e.3, g.3, h.3 and i.3) with all model configurations.

Table 5: Model evaluation metrics derived from the daily flow duration curve (April/1982-March/2015).

Metric	**Config.**	**Pocuro**	**Arrayán**	**Mapocho**	**Las Leñas**	**Claro**	**Colorado**	**Palos**	**Melado**	**Ñuble**
%BiasFMS	No Bands (NB)	15.5	21.6	22.6	53.4	45.8	5.2	52.9	31.2	59.9
	1000 m	17.6	25.3	22.1	47.3	46.0	4.7	50.1	27.8	57.7
	750 m	16.0	23.2	20.8	46.5	46.1	4.8	50.8	27.4	57.3
	500 m	16.7	23.2	22.3	45.8	45.4	4.7	49.3	25.9	55.8
	200 m	16.9	24.1	22.4	45.1	45.5	4.4	48.4	24.9	56.0
	100 m	17.4	23.9	22.2	45.2	45.4	4.5	47.8	24.8	55.6
%BiasFLV	No Bands (NB)	2.0	5.4	6.9	6.5	14.4	0.8	6.3	14.2	16.1
	1000 m	2.0	5.3	7.2	5.7	14.3	0.8	6.2	13.6	15.9
	750 m	1.9	5.2	6.9	5.6	14.3	0.8	6.2	13.6	15.9
	500 m	2.0	5.2	7.1	5.5	14.2	0.7	6.1	13.4	15.8
	200 m	2.0	5.1	7.0	5.5	14.2	0.7	6.0	13.2	15.7
	100 m	2.0	5.1	7.1	5.5	14.2	0.7	6.0	13.1	15.7

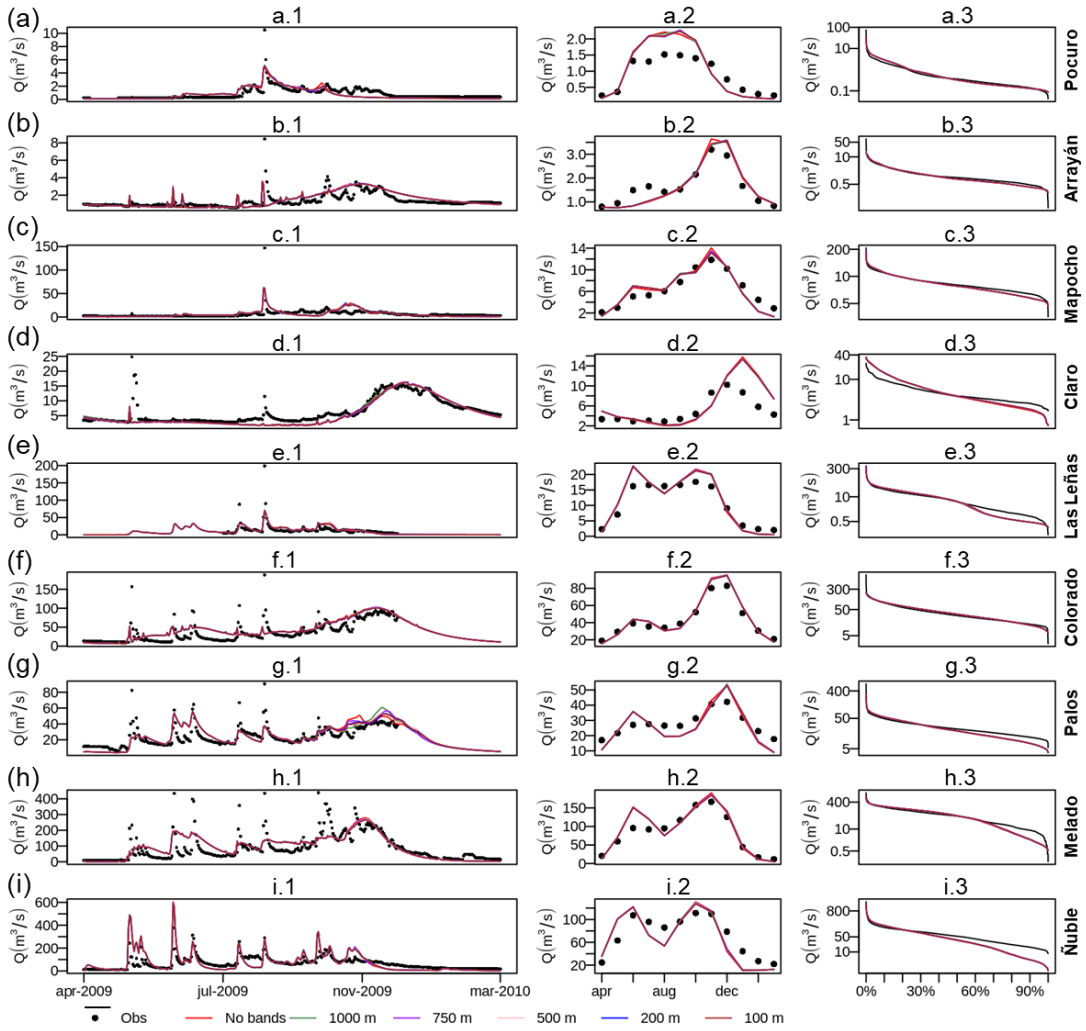

Figure 3. Comparison between simulated and observed runoff (Q) for all basins in terms of daily time series (April/2009-March/2010, left panels), mean monthly runoff (center panels) and daily flow duration curves (right panels). The results in center and right panels correspond to the climatological period. In the left panels, missing dots indicate the absence of runoff measurements.

Figure 4 illustrates the sensitivity of KGE to the configuration of elevation bands across basins and analysis periods, for daily (top panels) and monthly (bottom panels) runoff. In general, these results reinforce the idea that adding elevation bands has marginal effects on simulated basin-averaged runoff, yielding KGE improvements (i.e., ΔKGE) during the 5-year wet period that range from 0 to 0.05 (Palos basin) for both daily (Figure 4a) and monthly (Figure 4d) time scales. During the 5-year dry period (Figures 4b and 4e), the overall KGE improvement (average from all catchments) is 0.02, with the largest increments obtained for the Palos and Mapocho River basins (although the resulting KGE is still low), and negligible variations (~0.01) in the remaining basins.

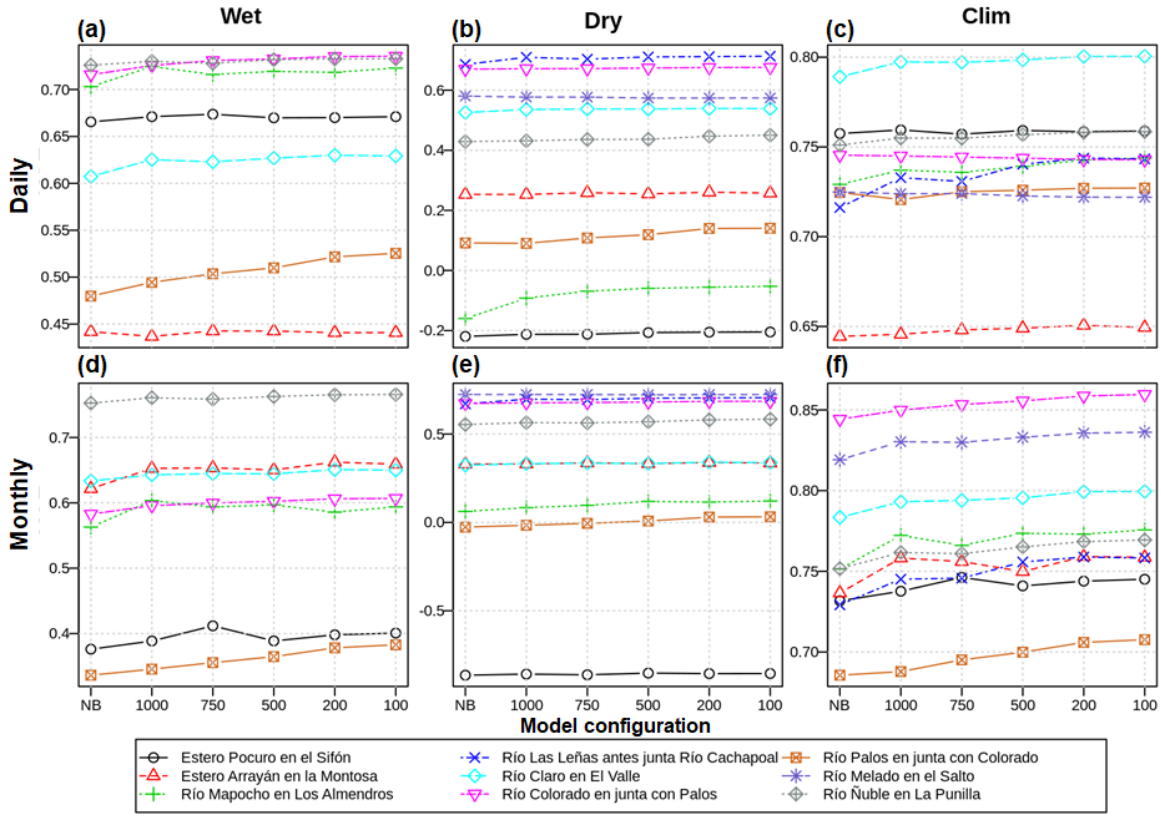

Figure 4. KGE results computed with daily (top) and monthly (bottom) runoff, obtained from the benchmark (NB: No Bands) and the five alternative model configurations (i.e., using 1000-m, 750-m, 500-m, 200-m, and 100-m elevation bands). Each curve displays individual basin results, and missing basins in some panels indicate the absence of verification (i.e., observed) data for that period.

During the climatological period (Figures 4c and 4f), similar performance metrics are obtained for the 200-m and 100-m configurations. For daily runoff simulations (Figure 4c), adding elevation bands provides KGE improvements ranging 0.02-0.03 in Las Leñas and Mapocho basins, and slight KGE reductions (less than 0.01) in Colorado and Melado basins. KGE values obtained from monthly runoff simulations (Figure 4f) increase between 0.01 and 0.03 in all basins when 200-m and 100-m configurations are used.

The results displayed in Figure 4 show that incorporating elevation bands generally yields improvements in streamflow simulations in terms of KGE; however, a higher vertical resolution does not necessarily translate into increased KGE in all basins (e.g. see results for Estero Arrayán in Figures 4a, 4b and 4c). A noteworthy result from Figure 4 is the constant, positive effect on KGE that adding elevation bands provides in the Palos River basin during the wet period, which may be explained by the linear shape of its hypsometric curve over most of its fractional area, favoring more evenly distributed areas across elevation bands. More generally, Figure 4 shows that the effects of increased vertical resolution are not necessarily linear, i.e., some 'coarse' model configurations provide better KGE results than configurations with more elevation bands, yet both configurations are an improvement

compared to the benchmark (see, for example, 750-m configuration results for the Pocuro basin in Figure 4d, and 1000-m configuration results of the Arrayán basin in Figure 4f). The analysis of KGE components (see Figures for Supplement S12, S13 and S14) reveals a similar behavior for these metrics, i.e., invariance of results with the choice of snow band configuration during the dry period, and changes in both wet and climatological periods. The largest impacts of alternative model configurations are obtained for the α component, with a moderate reduction.

The effects of adding elevation bands are somewhat different for NSE, for which improvements during the wet and climatological periods are greater than the response of KGE, especially in the Arrayán River basin. Further, negligible changes in NSE are observed during the dry period (Figure S3).

4.2. Effects on mean annual fluxes and September 1st SWE

Figure 5 illustrates the effects of adding elevation bands on simulated basin-averaged mean annual fluxes and SWE 09/01. Overall, changes in annual averages are smaller than 5% (with a few exceptions); differences between alternative configurations are usually smaller than differences between the benchmark and any model configuration with elevation bands; and the effects of increased vertical resolution are very small beyond 200-m. Further, variations produced by alternative model configurations are not necessarily proportional to the vertical resolution of elevation bands, and the sign of such impacts in a specific catchment may differ depending on the analysis period.

The alternative model configurations produce slight variations in mean annual runoff, with ~0.15% reductions during the wet and climatological periods in most basins. During the dry period, small reductions (<0.1%) are obtained in the Colorado, Melado and Ñuble River basins. The Arrayán River basin is the only catchment where the inclusion of elevation bands slightly increases (~0.5%) the mean annual runoff in all analysis. These small variations in mean annual runoff – compared to the other variables displayed in Figure 5 – suggest that the similarity in KGE values obtained for daily and monthly runoff with all model configurations (Figure 4) may be attributed to very different reasons. Indeed, mean annual rainfall decreases in seven catchments (i.e., all basins except Las Leñas and Mapocho) around 0.7-0.9% during the wet period, as the number of elevation bands increases. Very similar variations are observed during the dry and climatological periods; even more, the inclusion of more elevation bands also yields less rainfall during the dry period in the Mapocho River basin. Conversely, average increases of 2-3% in mean annual snowfall are obtained with the alternative model configurations.

The implementation of elevation bands results in mixed variations across catchments in basin-averaged SWE 09/01 with respect to the benchmark model. Negative changes are obtained in Las Leñas, Colorado and Ñuble River basins during all analysis periods; ~2% (~1%) less SWE 09/01 is observed in the Pocuro River basin during the wet period (the climatological period, using the 1000-m configuration); and small (<0.5%) negative variations in SWE 09/01 are obtained in the Palos River basin during the dry period. In the

remaining basins, more SWE 09/01 is simulated with the alternative model configurations, and variations depend on the analysis period and vertical discretization.

Interestingly, the results in Figure 5 show that more simulated snowfall does not necessarily yield more SWE 09/01. For example, adding elevation bands increases snowfall in the Colorado River basin in all analysis periods, producing less SWE 09/01 compared to the benchmark model. Additionally, all alternative configurations provide more snowfall in the Pocuro River basin; however more SWE 09/01 is obtained during the dry period, and less SWE 09/01 during the wet period.

Figure 5 also shows that incorporating subgrid elevation bands generally yields less snowmelt – with a few exceptions (i.e., Figures 5a.3, 5b.2, 5g.2, 5h.2) –, and mixed variations in annual sublimation amounts. Indeed, elevation bands tend to provide more sublimation in northern, water limited (i.e., PET/P >1) catchments (e.g., Figures 5a to 5d), and generally less sublimation in energy limited (i.e., PET/P <1) catchments basins. Slight increases (~0.6%) in simulated basin-averaged ET are obtained with the alternative model configurations during the wet (except Arrayán, with ~0.5% decreases) and climatological periods. During the dry period, the addition of elevation bands yields less simulated ET in four basins (Pocuro, Arrayán, Claro and Palos). For both ET fluxes and runoff, the results for sublimation, ET, snowmelt and runoff indicate that not all the basins show a clear relationship between the vertical discretization of elevation bands and variations in simulated annual fluxes with respect to the benchmark model (e.g., Figures 5g.1, 5g.2, 5h.1, 5h.2).

We now examine intra-catchment variability in changes induced by the alternative model configurations on simulated hydrological variables. Specifically, we assess percent changes [100*(alternative – benchmark)/benchmark] in simulated mean annual fluxes and SWE 09/01 at each grid cell across the Mapocho River basin (Figure 6). The same figures for the remaining catchments are in the supplementary information. It can be noted that the effects of elevation bands on mean annual rainfall are more evident in high elevation areas (over 3.000 m a.s.l.), where larger increments (all computed as the mean from the alternative configurations) are obtained during the wet period (~9% average) compared to the dry period (~2% average); additionally, rainfall increments are larger than 20% in some high-elevation grid cells during the wet period. Conversely, the incorporation of elevation bands yields less rainfall in low elevation grid cells, with declines < 5%.

As expected, simulated snowfall increases in grid cells located below 2,500 m a.s.l. when elevation bands are included, with larger increments for higher vertical resolutions. Snowfall variations in low-elevation areas are larger during the wet period with all alternative model configurations, spanning +20-50%. Further, adding elevation bands in the Mapocho River basin decreases snowfall amounts less than 10% in some grid cells located above 2.500 m a.s.l. The largest variations in SWE 09/01 generally occur below 3,000 m a.s.l., and these are more pronounced during the dry period; however, this behavior is not observed in the rest of the basins (see from Supplementary Figure S6 - Figure S11). Simulated annual sublimation and snowmelt can be largely affected by the inclusion of elevation bands. Interestingly, the sign and magnitude of snowmelt variations across does not necessarily match the spatial patterns of changes in SWE 09/01. Finally, Figure 6 shows that the alternative model

configurations do not induce substantial changes in mean annual ET and runoff across the basin of interest, which is also observed in the remaining basins.

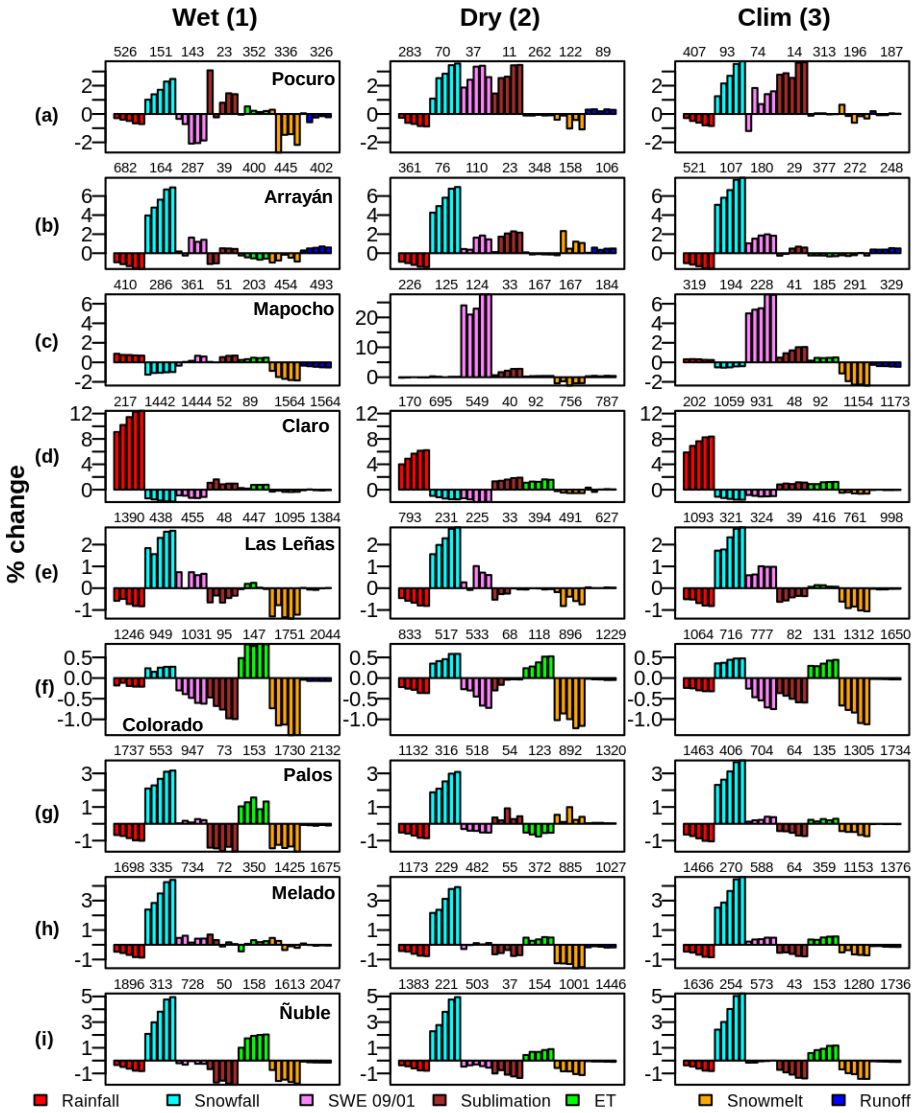

Figure 5. Percent changes [100*(alternative – benchmark)/benchmark] in simulated basin-averaged mean annual fluxes and SWE 09/01 for different periods (columns) and all case study basins. In each panel, the bars holding the same color represent, from left to right, percent changes for model configurations with 1000 m, 750 m, 500 m, 200 m and 100 m elevation bands. The numbers placed over each set of bars indicate the values obtained with the benchmark model. Note a different axis range is used for the Mapocho River basin during the dry period (c), due to overaccumulation on a grid cell with glacierized area (not shown here) which affects simulated SWE 09/01.

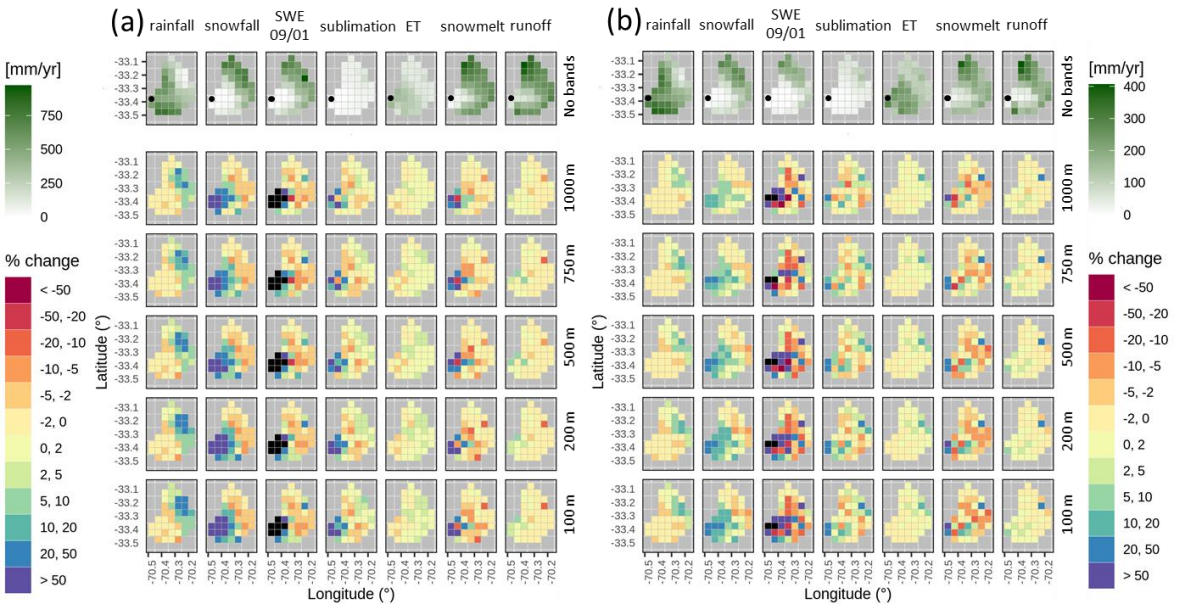

Figure 6. Spatial variability of percent changes [100*(alternative – benchmark)/benchmark] in grid cell-scale simulated mean annual fluxes and SWE 09/01 at the Mapocho en Los Almendros River basin. Results are presented for (a) wet and (b) dry analysis periods. The various columns display, from left to right, results for mean annual rainfall, mean annual snowfall, mean SWE 09/01, mean annual sublimation, mean annual ET, mean annual snowmelt and mean annual runoff. The top row displays results for the benchmark model in mm/yr (excepting SWE 09/01, presented in mm), while the remaining rows show results for alternative model configurations (i.e., 1000, 750, 500, 200 and 100 m elevation bands, from top to bottom). Black tiles indicate no data, associated to benchmark model results equal to zero (or unbounded result).The black dot in the top row represents the catchment outlet.

4.3. Differences in simulated daily SWE

We examine simulations of daily SWE in three grid cells of the Mapocho River basin during WYs 1984 and 2012 (Figure 7), characterized by wet and dry conditions, respectively. Despite the inclusion of elevation bands, model simulations yield less SWE in all grid cells during WY 1984, and snow disappearance gets delayed in grid cells (2) and (3) compared to the benchmark model. In grid cell (1), this does not happen due to its high mean altitude (3699 m a.s.l), yielding snow bands with similar altitudes and, therefore, a similar timing of simulated snow accumulation and melt. During WY 2012, the alternative model configurations also provide less average SWE than the benchmark model, with specific effects on simulated accumulation and melt events. For example, the 100-m configuration yields the largest melt rates before October, although it provides the highest SWE compared to the other configurations; in grid cell (2), a precipitation event at the end of July/2012 produces snow accumulation only if elevation bands are considered, even though it gets quickly melted; in grid cell (3), the alternative configurations provide less maximum SWE (~20 mm in mid-June) than the benchmark model, despite they generate earlier (almost two weeks) snow accumulation and extend the snow season for more than a week in some cases.

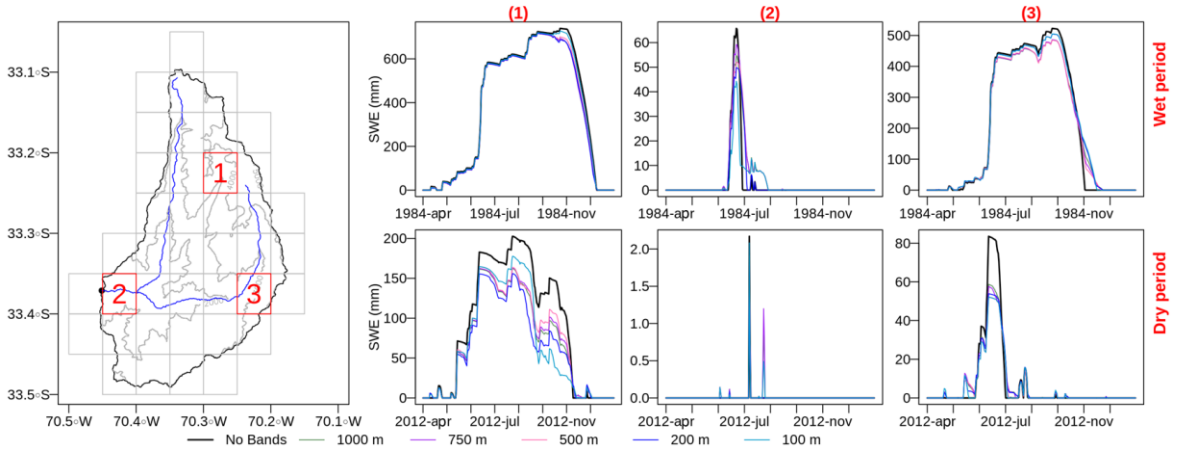

Figure 7. Simulated time series of daily SWE in three different grid cells across the Mapocho River basin (left panel), using the benchmark (black line) and alternative (colored lines) model configurations. The three rightmost columns display results for the selected grid cells, and two different water years associated to the wet (top panels) and dry (bottom panels) analysis periods.

Figure 8 shows time series of daily SWE simulated by individual elevation bands in grid cells (1), (2) and (3) (Figure 7), using 1000-m and 200-m configurations. It can be noted that differences between the benchmark model (red lines) and the spatial average of alternative configurations (black lines) are attributed to the appearance of SWE in low-elevation bands (gray lines). The comparison between 1000-m and 200-m simulations shows that adding more elevation bands enhances differences with the benchmark model; for example, the 1000-m (200-m) configuration yields 25 (39) mm less peak SWE than the benchmark in grid cell (1) during the dry period (Figure 8a). Further, the 200-m configuration yields larger seasonally-averaged SWE than the 1000-m configuration due to more snow accumulation at high elevations. Increasing the vertical resolution affects the seasonality of simulated SWE, with higher values in October 2012 using the 200-m configuration (Figure 8a, dry); indeed, the latter configuration provides a ~50 mm reduction in October 20 SWE compared to the benchmark model, while the 1000-m configuration reduces SWE for more than 80 mm the same day. This reveals another interesting feature: despite some high-elevation bands simulate more SWE than the benchmark model (see grey lines above the red line), this is not translated into increased spatially averaged SWE, due to their low contributing area.

In the low-elevation grid cell (Figure 8b), adding elevation bands yields a longer snow season, and the 200-m configuration enables more snow accumulation (compared to 1000-m), getting closer to the benchmark model results. Finally, the simulations for both (the 200-m) configurations during WY 1984 (WY 2012, after September) in grid cell (3) (Figure 8c) show that adding higher elevation bands can delay the occurrence of grid cell averaged snowmelt events. The highest elevation bands can start accumulating snow earlier during WY 2012, compared to the benchmark simulation.

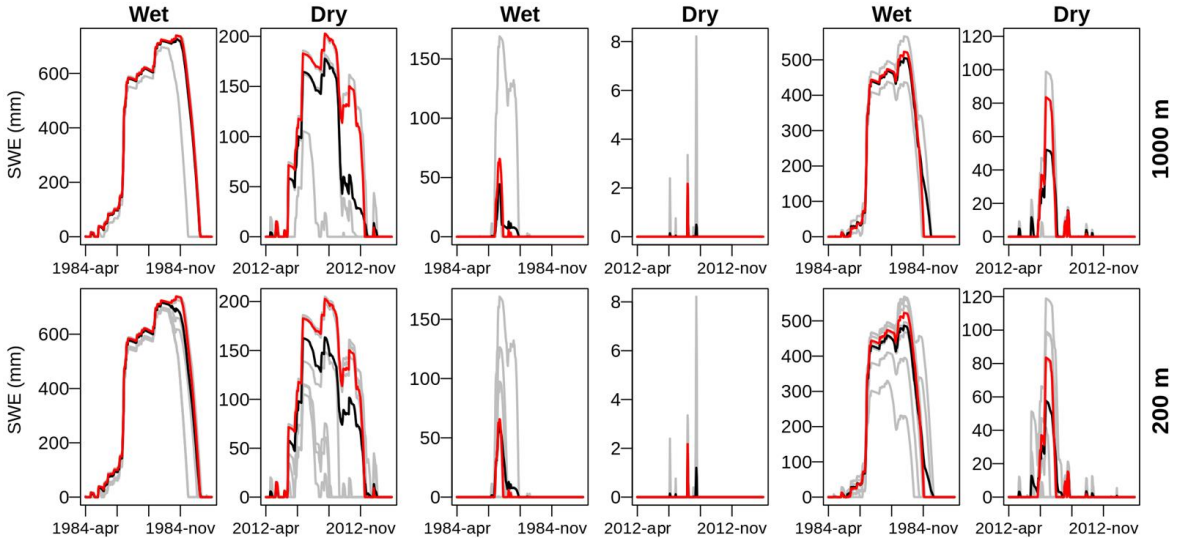

Figure 8, Comparison between simulated time series of daily SWE at the grid cell scale (i.e., ~0.05°) using the benchmark model (red line), vs. an alternative model configuration (black line) with elevation bands (Δz =1000 m, top panel; and Δz = 200 m, bottom panels) for selected grid cells (panels (a), (b) and (c) correspond to grid cells (1), (2) and (3) in Figure 7). In each panel, the gray lines show daily SWE simulated at each elevation band contained in the grid cell of interest. Each column displays results for a snow season belonging to the wet and dry subperiods.

4.4. Links between the effects of elevation bands and grid cell characteristics

The results in Figure 6 and Figures S4-S5-S7 show that adding elevation bands may have large effects on simulated SWE 09/01 in some grid cells, introducing considerable intra-catchment variability. Nevertheless, this variability compensates in such a way that implementing elevation bands yields smaller effects at the basin scale (Figure 9a), compared to the grid cell scale (i.e., ~0.05°) used here (Figure 9b). Hence, we now turn our attention to the question: where does the implementation of elevation bands make a larger difference in simulated SWE? To look for answers, we examine discrepancies between CDFs with attributes (defined according to section 3.3.3) of sensitive and insensitive grid cells (Figure 10). The results show that sensitive grid cells have lower mean elevations (median of 1700 m a.s.l.), larger elevation ranges and average slope, and smaller aspect in the range 120-240 (NW-SW) than insensitive ones. Further, sensitive grid cells show higher mean annual temperatures (median around 8°C compared to 6°C from insensitive grid cells), mean annual precipitation mostly over 1000 mm/yr (90% of sensitive grid cells), and a considerable fraction of precipitation falling as snowfall (the median f_s value of sensitive grid cells is 0.41, versus a median of 0.20 for insensitive grid cells). The annual average moisture index (I_m) and the moisture index seasonality (I_{mr}) are larger in sensitive grid cells, indicating more humid conditions and more pronounced intra-annual variations in meteorological conditions, switching from fully arid to fully saturated.

.

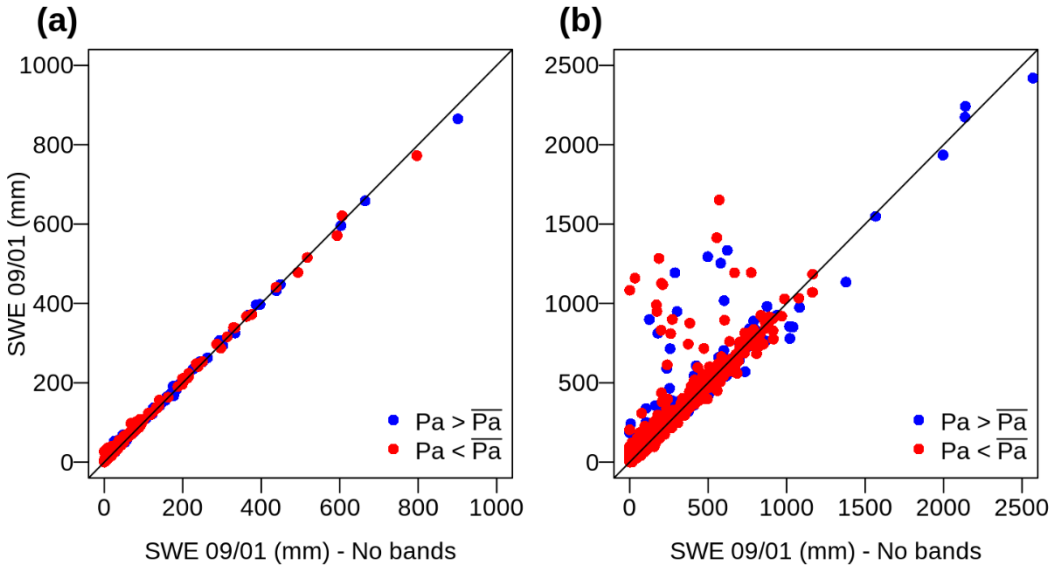

Figure 9. Simulated SWE 09/01 using 200-m elevation bands vs. the same variable obtained with the benchmark model at the (a) catchment scale, and (b) individual 0.05° grid cells. Each dot indicates results for a specific combination of water year and spatial unit, and each panel comprises results from all the grid cells contained in the nine case study basins. Results are stratified for dry (red) and wet (blue) water years, defined using the mean annual precipitation ($\overline{Pa}$) for the climatological period as threshold.

Figure 11 compares model states and fluxes simulated with 200-m elevation bands in sensitive and insensitive grid cells, showing that larger rainfall amounts – with median ~1500 mm/yr –are obtained in sensitive grid cells, compared to the median from insensitive grid cells, which is close to 1250 mm/yr; conversely, smaller snowfall amounts (with median ~190 mm/yr) are obtained in sensitive grid cells, compared to the median from insensitive grid cells (~330 mm/yr). Accordingly, lower values of maximum SWE are reached in sensitive grid cells (~370 mm) compared to insensitive grid cells (~590 mm/yr). This behavior is expected given the relatively lower mean elevation of sensitive grid cells (Figure 10). The results for annual snowmelt show large differences between the shape of the CDFs, similar to annual precipitation behavior (Figure 10). The sublimation of sensitive grid cells is higher (~60 mm/yr) compared to insensitive grid cells (~45 mm/yr), and the shapes of the CDFs are similar to the shapes obtained for maximum SWE. Annual runoff discrepancies between sensitive and insensitive CDFs are only noticeable for values smaller than 1600 mm/yr, with a relatively larger p-value. Finally, we do not find considerable differences in terms of ET between sensitive and insensitive grid cells.

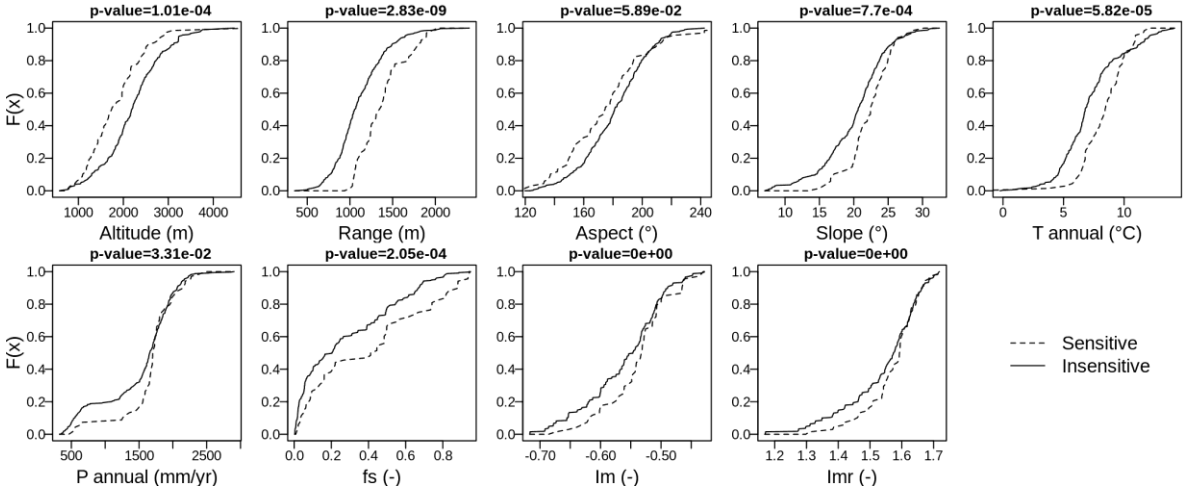

Figure 10: CDFs of selected physiographic and hydroclimatic attributes for sensitive vs. insensitive grid cells. Aspect values of 180º (90º) represent west (north) facing grid cells. We identify grid cells as sensitive grid if differences in simulated SWE 09/01 with respect to the benchmark model are larger than 10% for >50% of water years in the climatological period. The p-value is obtained from applying the Kolmogorov-Smirnov test between sensitive and insensitive groups. The results were obtained using the 200-m configuration.

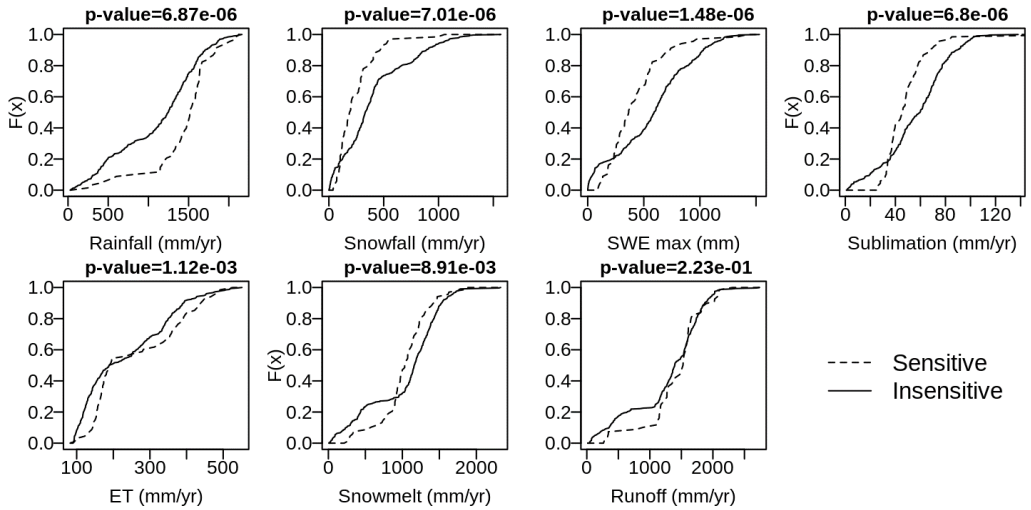

Figure 11: Same as in Figure 10, but for model states and fluxes simulated with 200-m elevation bands.

5. Discussion

The results presented in this paper unveil several implications that the delineation of elevation bands may have on hydrological characterizations, including streamflow performance metrics. Indeed, the KGE results for daily and monthly streamflow (Table 4) do not differ considerably among the model configurations tested here. The maximum KGE improvement

provided by alternative model configurations (compared to the benchmark) is ΔKGE = 0.03 for the Mapocho and Palos River basins, which cannot be considered an improvement in streamflow due to the inclusion of snow bands (Clark et al., 2021). These small changes suggest a form of model-structure-equifinality for KGE (Khatami et al., 2019), since spatial heterogeneities arising from different modeling alternatives compensate to produce very similar values for the same performance metric applied at the catchment scale. This is not observed, however, when analyzing the bias in the FDC mid-segment slope (%BiasFMS). For Las Leñas and Palos River basins, the bias reductions (100-m – benchmark) are 8.2% and 6.4% respectively. A reduction for the same metric is obtained in the remaining basins when comparing the 100-m configuration with the benchmark, excepting the Arrayán River basin, where the bias increases 2.3%. For the FDC low-segment volume (%BiasFLV), small variations (<1.1%) are obtained.

Despite the little differences among alternative configurations for KGE (and its components) and NSE, we found notable discrepancies in simulated basin-averaged variables, and spatial differences in rainfall, snowfall, SWE 09/01, sublimation, ET, snowmelt and runoff compared to the benchmark model (Figure 6). In general, smaller variations in simulated hydrological variables are obtained as more elevation bands are added – especially beyond a 200-m vertical resolution –, in agreement with past studies (e.g., Essery, 2003; Pradhanang et al., 2011; Bhatta et al., 2019). Interestingly, the direction (i.e., sign) of variations introduced by elevation bands (compared to the benchmark) is not the same for all catchments and type (i.e., wet/dry) of the analysis period.

As expected, simulated processes (i.e., precipitation partitioning into snowfall and rainfall, daily SWE) vary when vertical heterogeneity through vertical air temperature gradient is included, and generally the effects increase with vertical resolution. Such heterogeneity causes differences in snow accumulation across elevation bands, decreasing spatially-averaged peak SWE in each grid cell and delaying snow cover depletion (Figure 9). This aligns well with the findings of Essery (2003), who concluded that the aggregated model (equivalent to our benchmark model) was unable to represent winter melt at low elevations and delayed spring melt at high elevations. Other studies have also highlighted the role of sub-grid heterogeneity for more realistic SWE calculations, and therefore for improved snowmelt water estimates (e.g., Clark et al., 2011; DeBeer & Pomeroy, 2017). Our results also show that low elevation bands accumulate less SWE and melt earlier – in agreement with observations reported by Tong et al. (2008) for a watershed in western Canada –, while the highest elevation bands yield lower melt rates, reducing the snow cover depletion rate (i.e., snow last longer). Such difference can be explained by changes in the energy balance (specifically, sensible heat fluxes, latent heat fluxes and turbulent fluxes, Figures S15-S23) since, in our configuration, precipitation is spatially uniform in each grid cell with all model configurations.

A novel contribution of our study is the identification of physiographic and climatic controls defining where it is more important to incorporate elevation bands. Our results clearly demonstrate that topographic attributes play a key role, including elevation range, and spatially-averaged elevation and slope. Despite we did not find statistically significant differences (i.e., p-value > 5%) in terms of aspect between insensitive and sensitive grid cells, the sensitive grid cells group was found to follow a northern orientation. This connection

between low elevation and aspect aligns well with the findings of Helfricht et al. (2012), who examined LiDAR observations acquired at the Upper Rofen valley in Austria, concluding that south-facing (equivalent to north-facing in the Southern Hemisphere) exposed slopes at the lowest elevation bands remain almost snow free at the end of 2001, 2002 and 2008 accumulation periods, due to high radiation loads.

A key limitation of this study is that subgrid variability in precipitation was not explicitly incorporated (Pradhanang et al., 2011; Grusson et al., 2015). Hence, future work could expand these analyses to account for orographic controls on precipitation, as well as incoming radiation fluxes or other meteorological forcings, and examine implications on energy balance fluxes. Because the strategy to delineate snow bands should prioritize a proper representation of SWE at those altitudes with the largest areas, showing high snow accumulation (Helfricht et al., 2012), the effectiveness of irregular vertical discretizations could be tested to emphasize the importance of such areas. Additionally, it would be useful to assess the effects of different elevation band configurations on streamflow forecasts or projected climate change impacts on hydrological variables, including case studies from other snow climates (as in Raleigh et al., 2015) and even simpler (e.g., conceptual, bucket style) hydrologic models.

6. Conclusions

We have examined the hydrological implications of representing subgrid variability through elevation bands in nine basins located along the western slopes of the Andes Cordillera. Specifically, we implemented five alternative model configurations in the VIC macro-scale hydrological model, with elevation bands every 1000, 750, 500, 200 and 100 m, and compared their results against a benchmark model (i.e., model without elevation bands) in terms of streamflow simulations, mean annual fluxes and SWE 09/01, and daily SWE simulations in a suite of grid cells located across the Mapocho River basin. Finally, we analyzed possible physical and climatic characteristics that define those grid cells where elevation bands are more impactful on SWE estimates. The results show that, although the incorporation of elevation bands does not appreciably affect model performance in terms of the Kling-Gupta efficiency for daily or monthly streamflow, it does affect other fluxes and SWE at the catchment scale and the intra-basin variability of simulated variables, suggesting a kind of model-structure-equifinality. Other findings are as follows:

- Elevation bands yield larger effects in the partitioning of precipitation into rainfall and snowfall, for both catchment and grid cell scales – during the wet period (WYs 1982-1986) compared to the dry period. Additionally, differences in ET and runoff between the alternative model configurations and the benchmark are also more pronounced during the wet period, although not as evident as the case of rainfall and snowfall. On the other hand, impacts of vertical discretization on SWE 09/01 are comparatively more relevant during dry periods.
- Adding elevation bands generally yields less basin-averaged snowmelt, and more (less) catchment-scale sublimation across water-limited (energy-limited) basins.

- The magnitude of variations in simulated hydrological variables induced by elevation bands is not proportional to the vertical discretization or number of elevation bands adopted.
- Adding elevation bands affects the duration of snow cover – with the highest bands holding snow for a longer period –, and yields earlier snow accumulation during the water year compared to the benchmark model.
- SWE 09/01 is generally more affected by elevation bands in grid cells with relatively lower mean altitude, elevation ranges >1000 m, steep slopes (>15°) and annual precipitation amounts <1000 mm that occur within a few months.

Acknowledgments

This research/thesis was partially supported by the supercomputing infrastructure of the NLHPC (ECM-02). Pablo A. Mendoza received support from Fondecyt Project 11200142 and CONICYT/PIA Project AFB180004.

Supplement

Table shows the attributes used in this study for basin selection, including the glacier area, the intervention degree (relationship between annual volume of water assigned as permanent consumptive rights and the mean annual flow) and the presence of big dams.

Table S1: Attributes for the case study basins included here, and used for the catchment selection process (Alvarez-Garreton et al., 2018).

Catchment	Glacier area (%)	Intervention degree (%)	Big dams
Estero Pocuro en el Sifón	0	0	No
Estero Arrayán en la Montosa	0	5.78	No
Río Mapocho en Los Almendros	0.73	0.27	No
Río Las Leñas antes junta Río Cachapoal	0.45	0	No
Río Claro en El Valle	0	0.05	No
Río Colorado en junta con Palos	0.72	0	No
Río Palos en junta con Colorado	0.02	< 0.01	No
Río Melado en el Salto	0.97	< 0.01	No
Río Ñuble en La Punilla	1.09	0.26	No

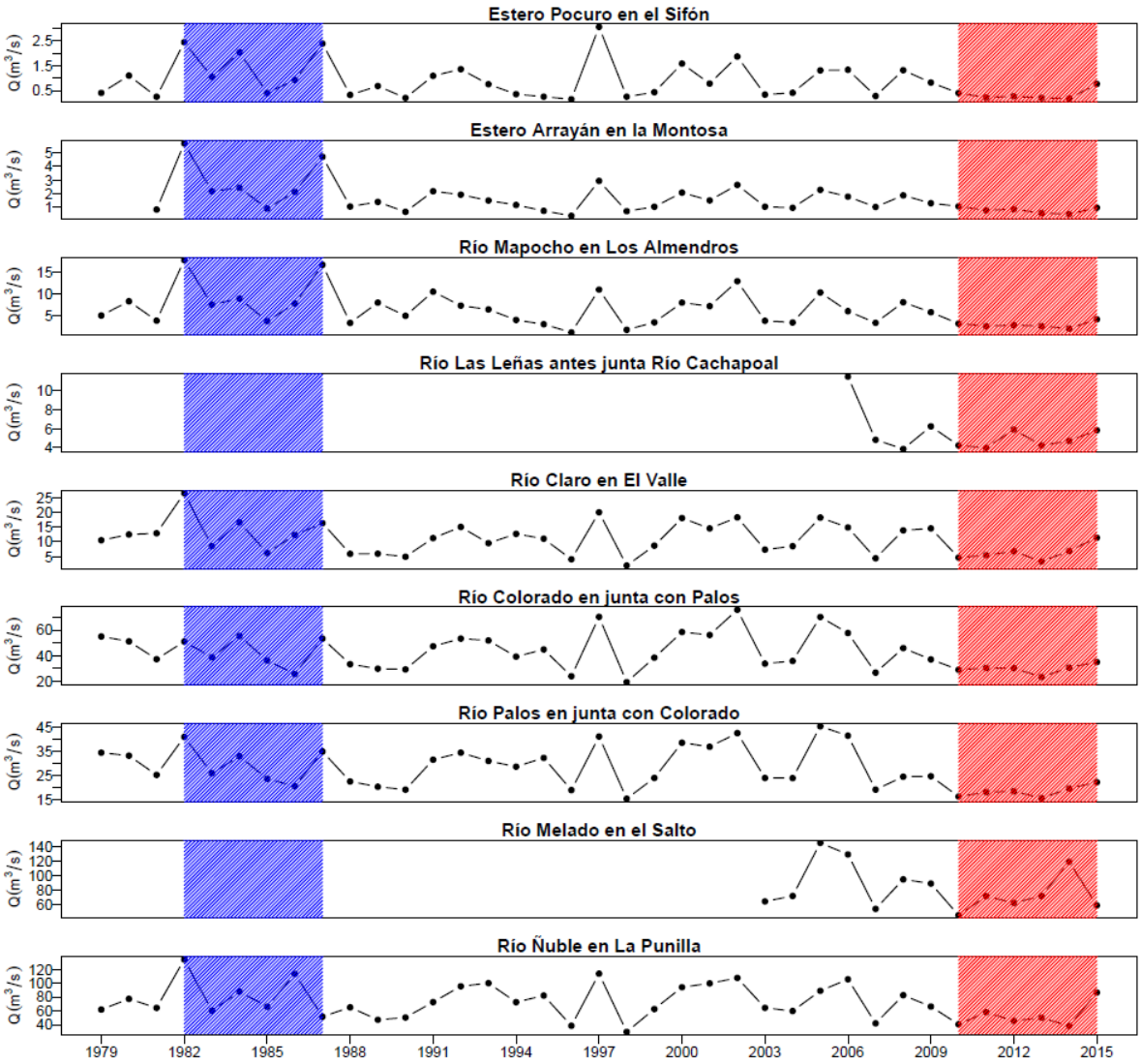

Figure S1: Time series of mean annual streamflow for the climatological period. The blue shaded region represents the wet period (April/1982 – March/1986). Red shaded subperiod represents dry period (April/2010 – March/2014).

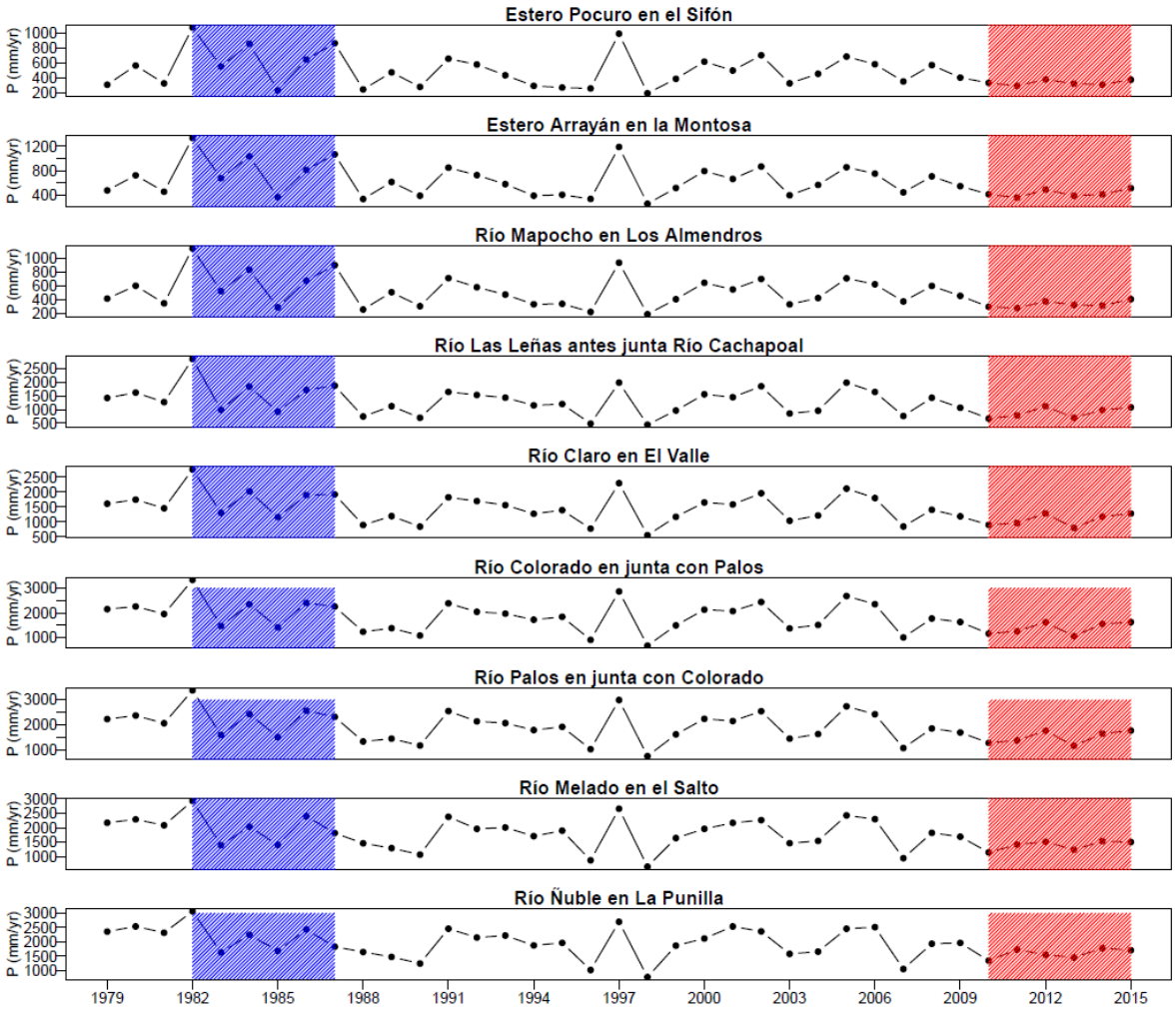

Figure S2: Time series of annual precipitation for the climatological period. The blue shaded region represents the wet period (April/1982 – March/1986). Red shaded subperiod represents dry period (April/2010 – March/2014).

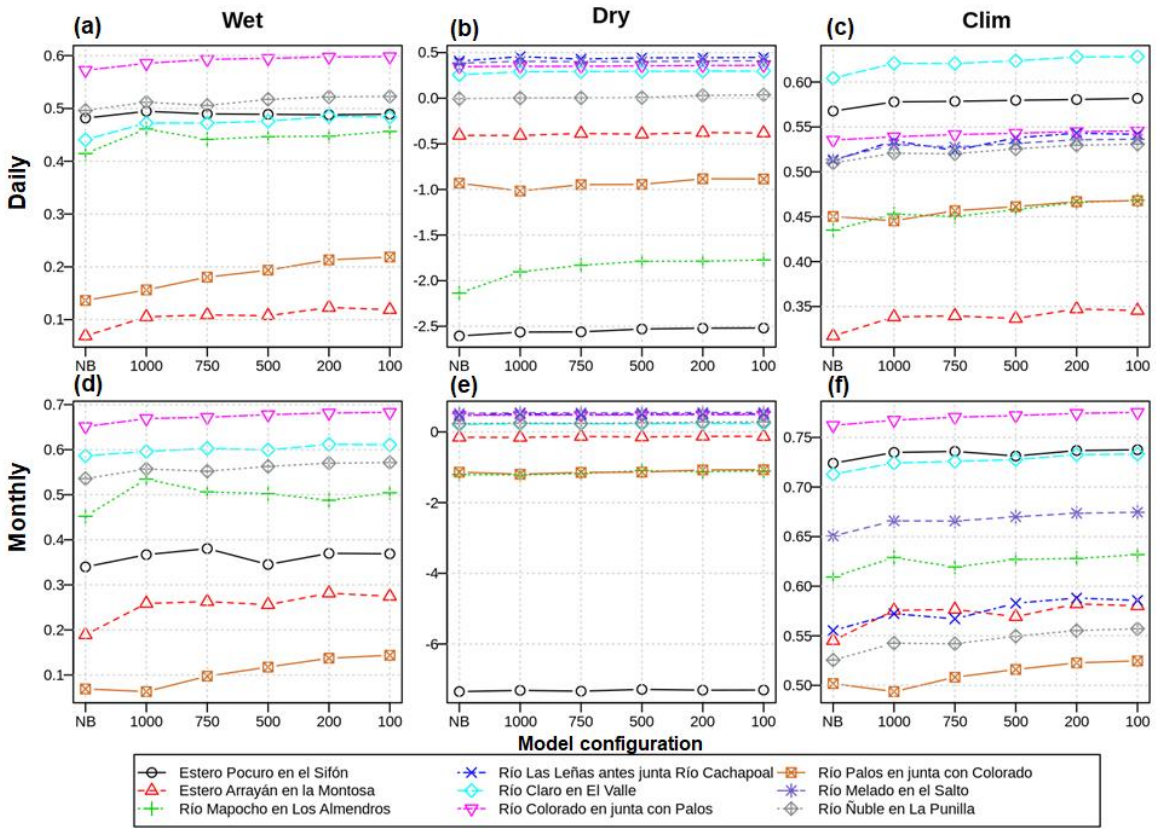

Figure S3: NSE results computed with daily (top) and monthly (bottom) runoff, obtained from the benchmark (NB: No Bands) and the five alternative model configurations (i.e., using 1000-m, 750-m, 500-m, 200-m, and 100-m elevation bands). Each curve displays individual basin results, and missing basins in some panels indicate the absence of verification (i.e., observed) data for that period.

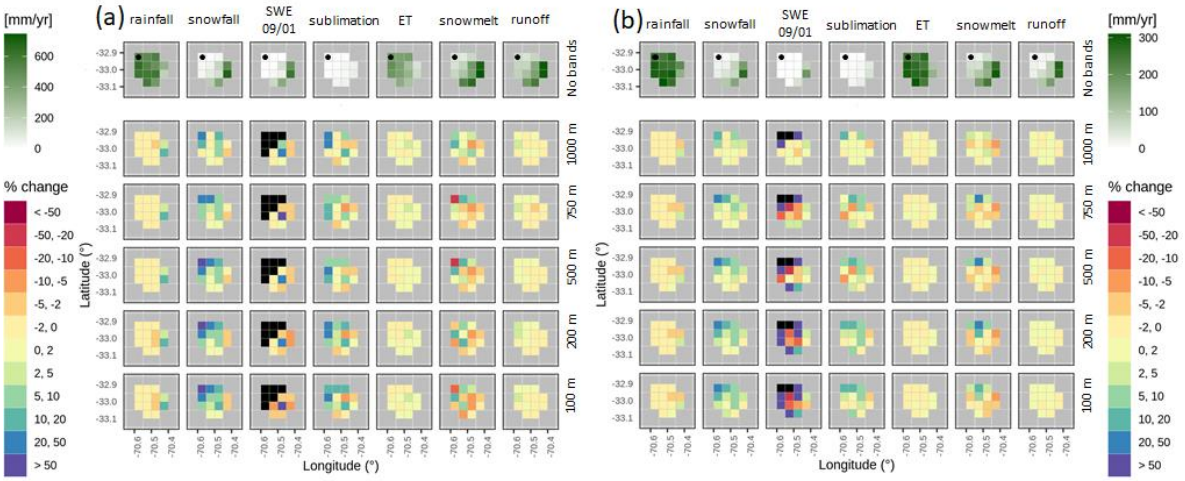

Figure S4: Spatial variability of percent changes [100*(alternative – benchmark)/benchmark] in grid cell-scale simulated mean annual fluxes and SWE 09/01 at the Pocuro en el Sifón basin. Results are presented for (a) wet and (b) dry analysis periods. The various columns display, from left to right, mean annual rainfall, mean annual snowfall, mean SWE 09/01, mean annual sublimation, mean annual ET, mean annual snowmelt and mean annual runoff. The top row displays results for the benchmark model in mm/yr (excepting SWE 09/01, presented in mm), while the remaining rows show results for alternative model configurations (i.e., 1000, 750, 500, 200 and 100 m elevation bands, from top to bottom). Black tiles indicate no data, associated to benchmark model results equal to zero (or unbounded result). The black dot in the top row represents the catchment outlet.

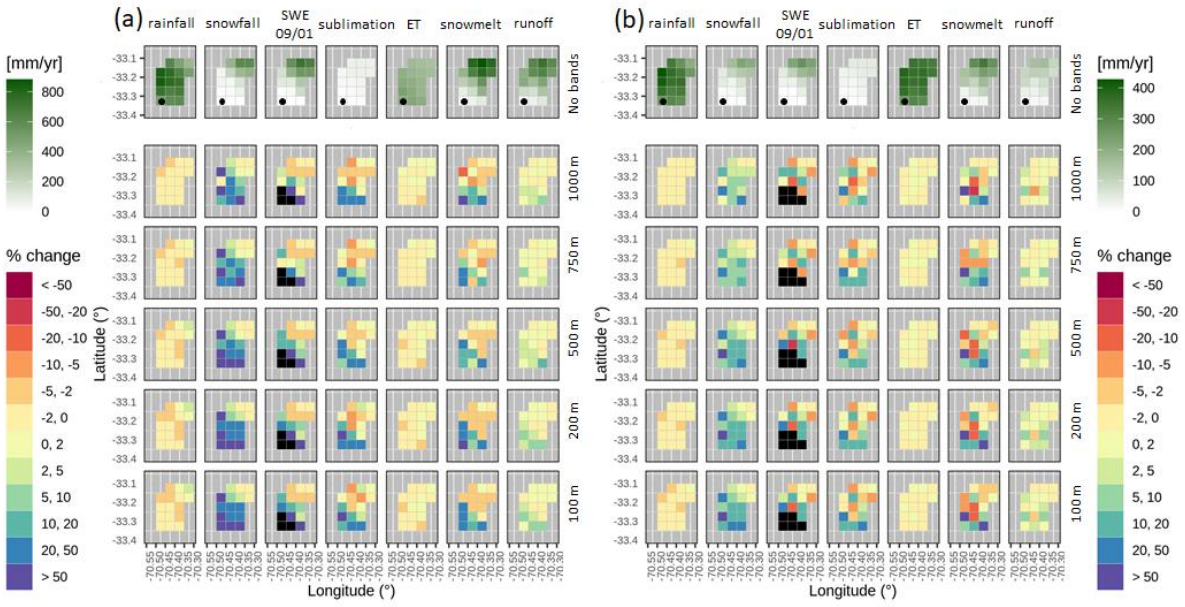

Figure S5: Same as in Figure S4, but for Estero Arrayán en la Montosa

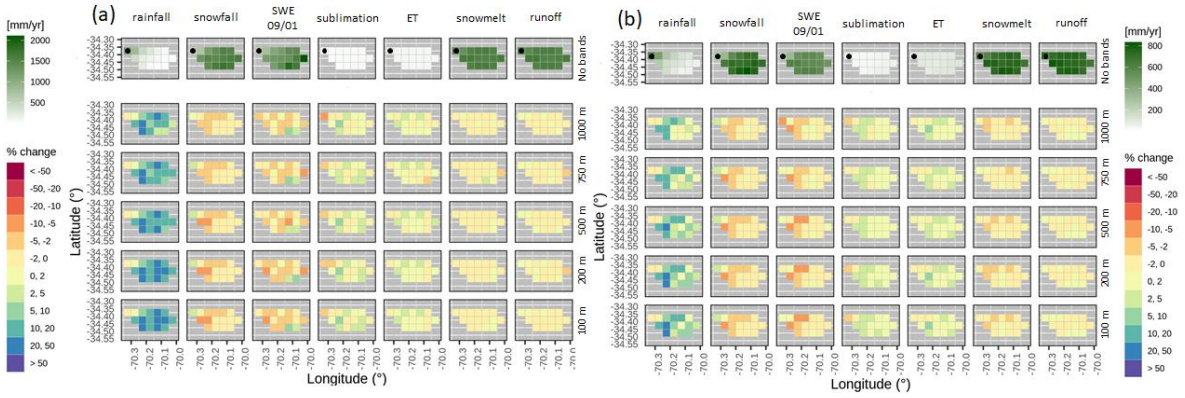

Figure S6: Same as in Figure S4, but for Las Leñas antes junta Río Cachapoal

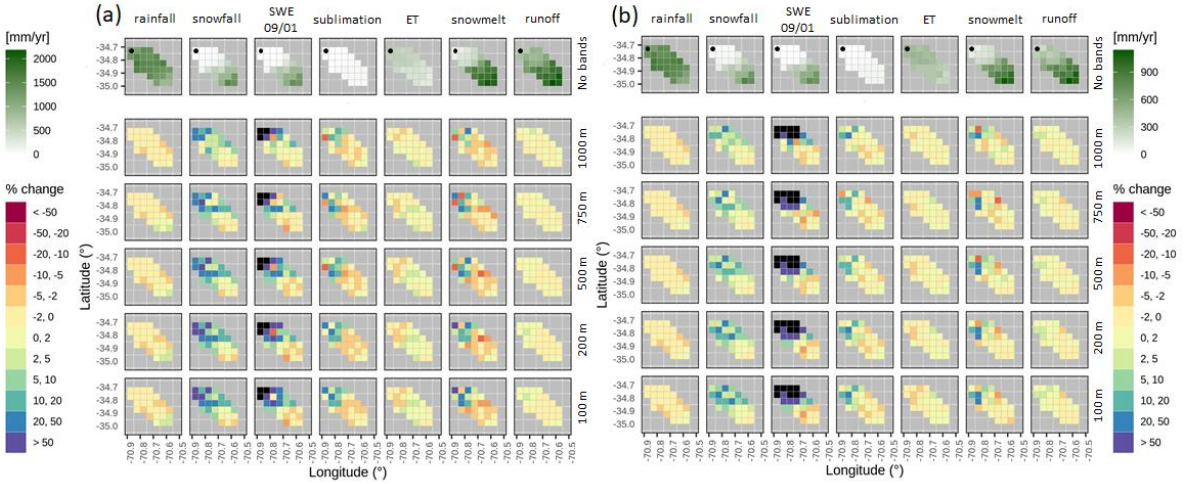

Figure S7: Same as in Figure S4, but for Río Claro en El Valle.

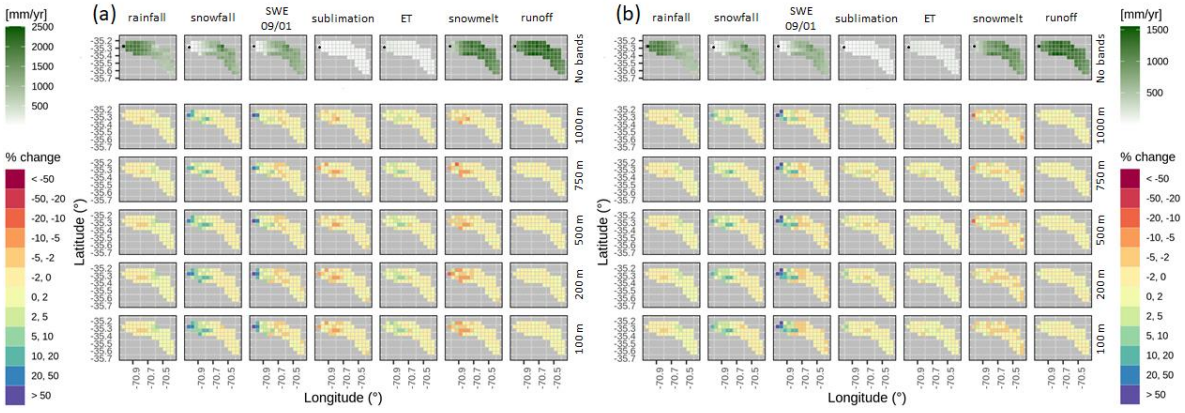

Figure S8: Same as in Figure S4, but for Río Colorado en junta con Palos.

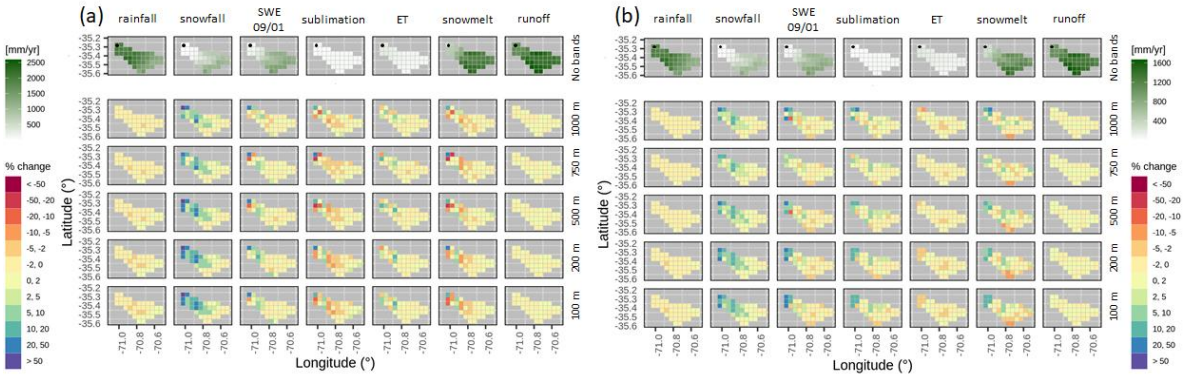

Figure S9: Same as in Figure S4, but for Río Palos en junta con Colorado.

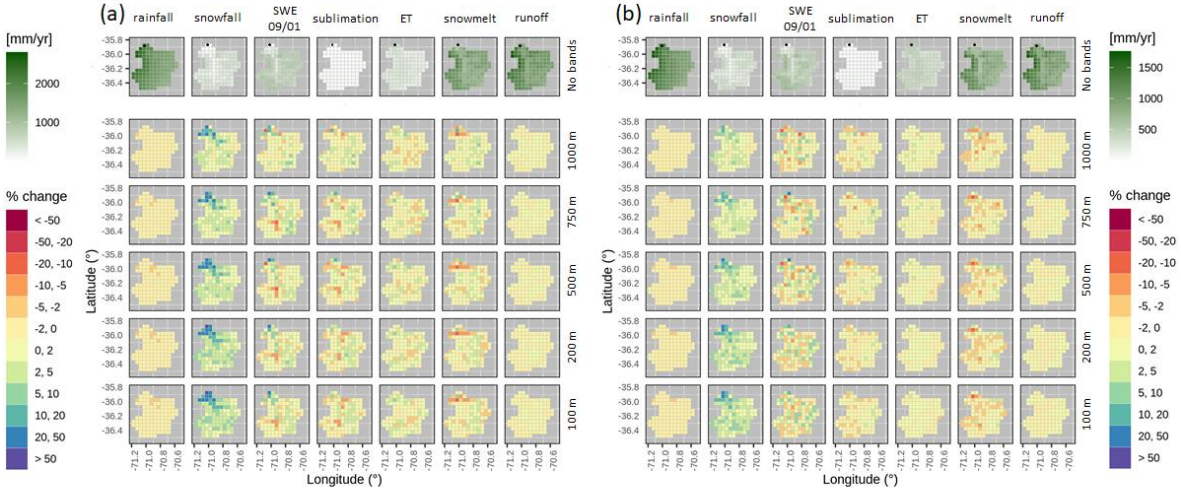

Figure S10: Same as in Figure S4, but for Río Melado en El Salto.

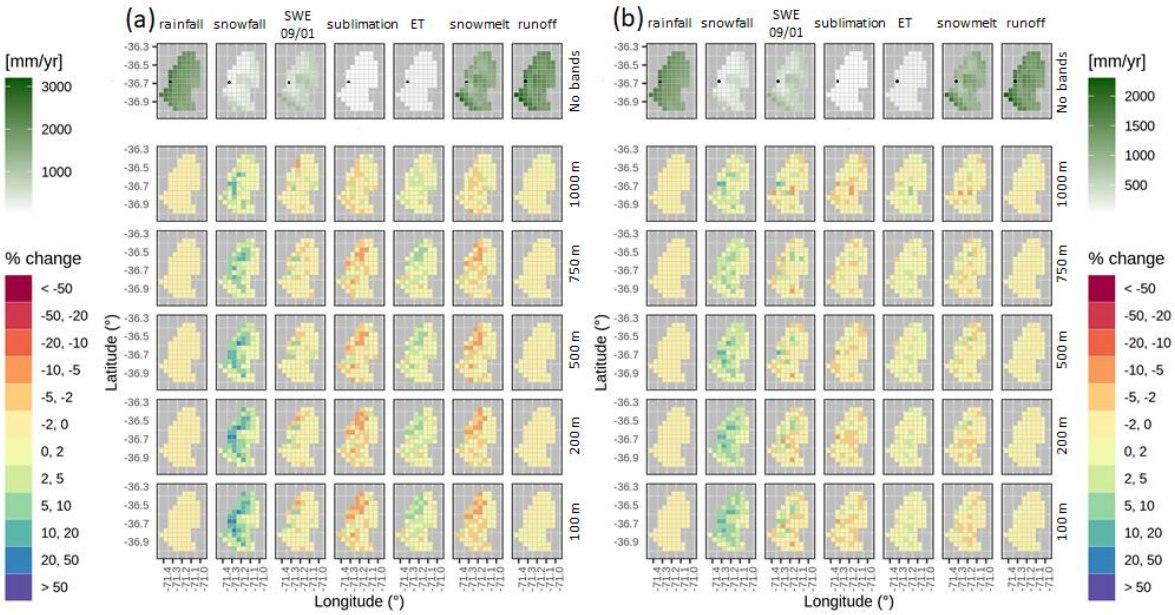

Figure S11: Same as in Figure S4, but for Río Ñuble en La Punilla.

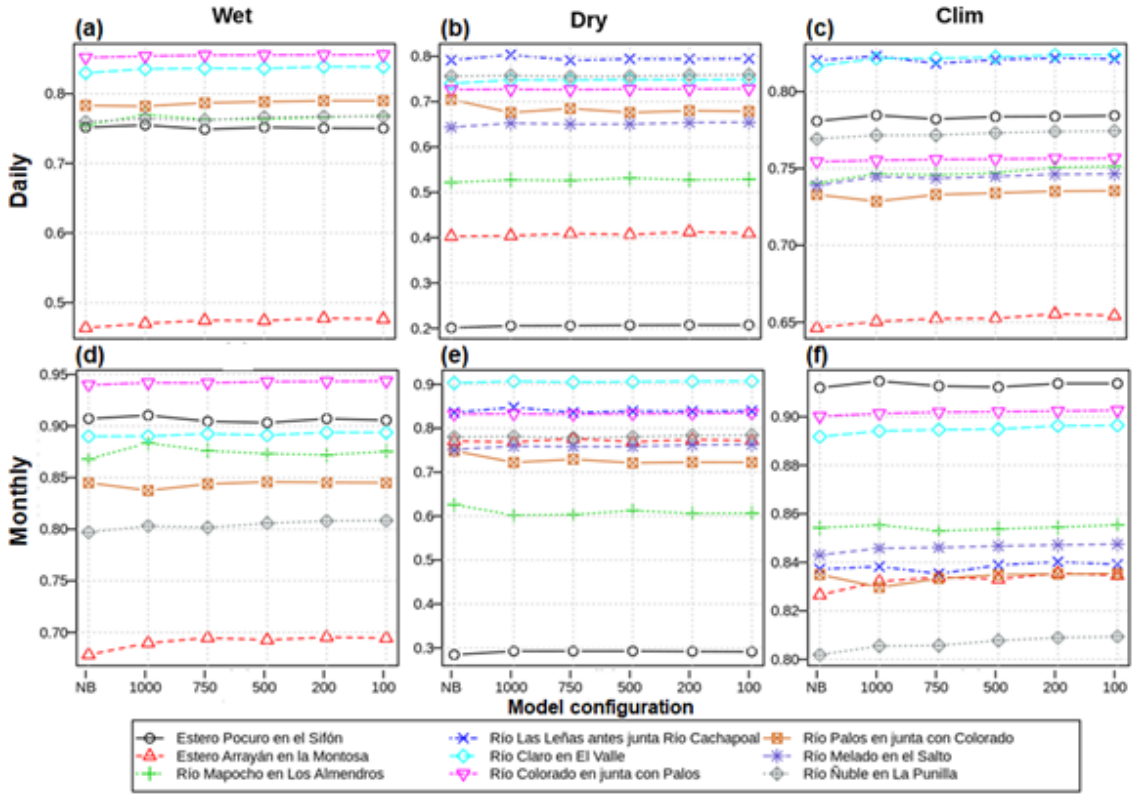

Figure S12: Pearson product-moment correlation coefficient between simulated and observed runoff. The results are displayed for daily (top) and monthly (bottom) runoff, obtained from the benchmark (NB: No Bands) and the five alternative model configurations (i.e., using 1000-m, 750-m, 500-m, 200-m, and 100-m elevation bands). Each curve displays individual basin results, and missing basins in some panels indicate the absence of verification (i.e., observed) data for that period.

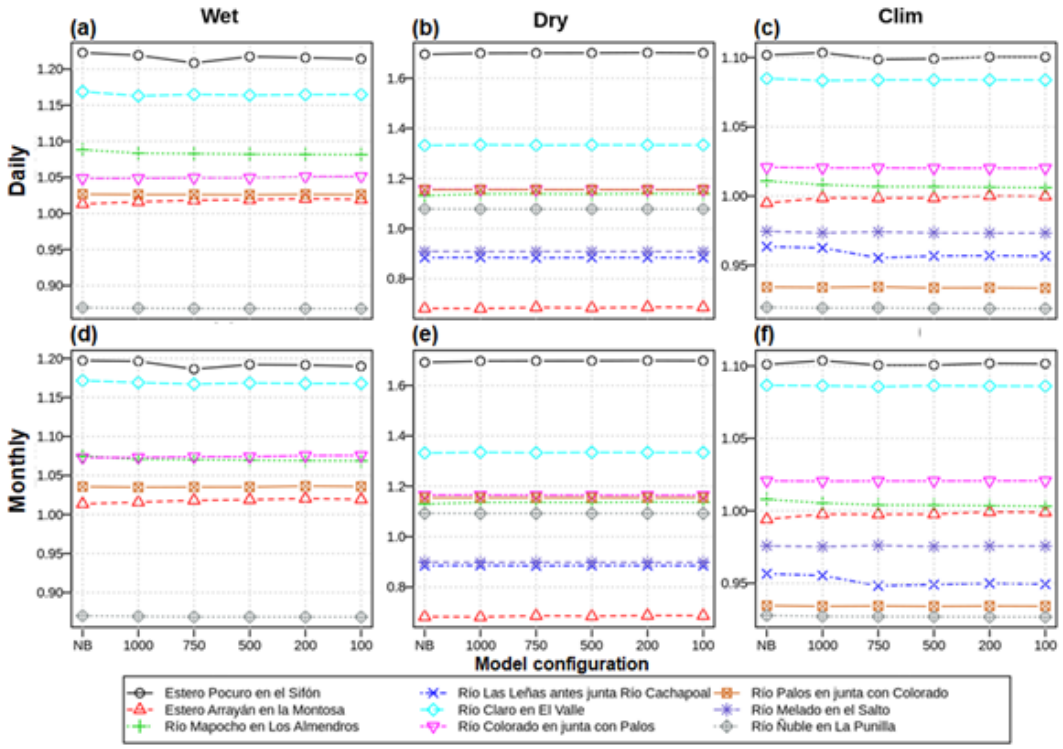

Figure S13: Same as in Figure S12, but for the ratio β between the mean of the simulated values to the mean of observations.

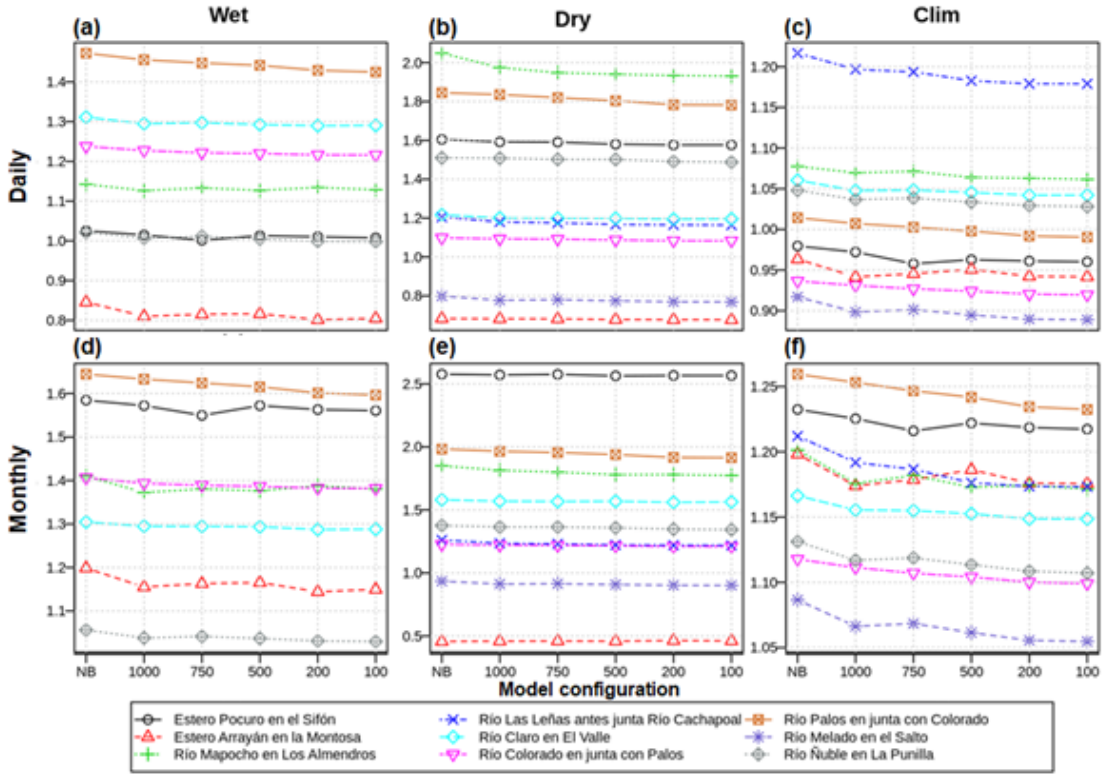

Figure S14: Same as in Figure S12, but for the ratio α of the standard deviation of simulated values to the standard deviation of observed values.

Energy Balance

In this section, we provide details on the energy balance approach implemented in VIC, and the results obtained for the basins of interest.

VIC computes the albedo using the United States Army Corps of Engineers method (USACE, 1956), which is an empirical equation for albedo decay, where this variable depends on the age of snow surface. Therefore, snow albedo is not directly affected by air temperature.

In VIC, the cloudiness and its effect on radiation is calculated using equations 2.29 from Bras (1990) and the method of Deardorff (1978). Part of the code used by VIC for processing atmospheric data comes from MT-CLIM, which is a weather preprocessor developed by the NTSG group in the School of Forestry at the University of Montana.

The longwave radiation, which can be succinctly described in terms of an emissivity, was calculated using the Prata parametrization (1996):

$$\varepsilon = 1 - (1 + \xi)\exp\left(-\sqrt{1.2 + 3.0\xi}\right) \quad (4)$$

$$\xi = \left(\frac{e_0}{T_0}\right)\left(\frac{M_w}{R^* k \psi}\right) \quad (5)$$

$$\psi = 1 + \overline{\left(\frac{e}{p}\right)}\frac{M_w}{M_a} \quad (6)$$

$$k = k_w + \frac{\gamma}{T_0} \quad (7)$$

where:
ε: clear-sky emissivity
e_0: screen-level value of the vapor pressure.
e: partial pressure of water vapor.
T_0: measured temperature.
γ: temperature lapse rate.
M_w and M_a are the molecular weight of water vapor and dry air, respectively.
R^*: universal gas constant ($R^* = 8.314 \cdot 10^3 Jkg^{-1}kmol^{-1}$)

In equation (6), the overbar represents de mean value.

The incident solar radiation is obtained iteratively, using the equations by Thornton & Running (1999).

Canopy temperature is obtained by iteratively solving the canopy-atmosphere and canopy-ground exchange fluxes (e.g., turbulent fluxes).

Figures S15-S23 show the spatial heterogeneity obtained with the benchmark model for the net radiation at the surface (including longwave and shortwave radiation), latent and sensible heat fluxes from the surface and the ground heat flux plus heat storage in the top soil layer.

Additionally, the intra-catchment variability of changes induced by different subgrid discretizations is also illustrated. The key findings of these figures are as follows:

- In general, the results show that incorporating elevation bands does not yield variations of net radiation larger than 10% in any basin, during both analysis periods. Further, the effects of increasing the number of elevation bands in all basins seem to be moderate.

- In some basins, the latent heat flux gets reduced near the catchment outlets (e.g. Figures Figure S15a, Figure S17a, Figure S19a, Figure S21b), while in others larger reductions are obtained at high elevations (e.g. Figures Figure S20a, Figure S21a, Figure S23a). In general, elevation bands provide the largest variations for this variable during the wet period.

- The results show that elevation bands yield reductions in sensible heat flux at the highest altitude grid cells (e.g. Figures Figure S15, Figure S18). Again, the largest variations occur during the wet period (specially in Las Leñas basin, Figure S18).

- Finally, elevation bands yield increased ground heat flux near the catchment outlets, and also reductions that mostly occur in high elevation grid cells (e.g., Figures Figure S15, Figure S17b, Figure S19, Figure S21b). For some basins and configurations, the largest decrease in ground heat flux is obtained at the lowest altitude grid cell (e.g., Figures Figure S16a, Figure S17a, Figure S18, Figure S19a, Figure S21a).

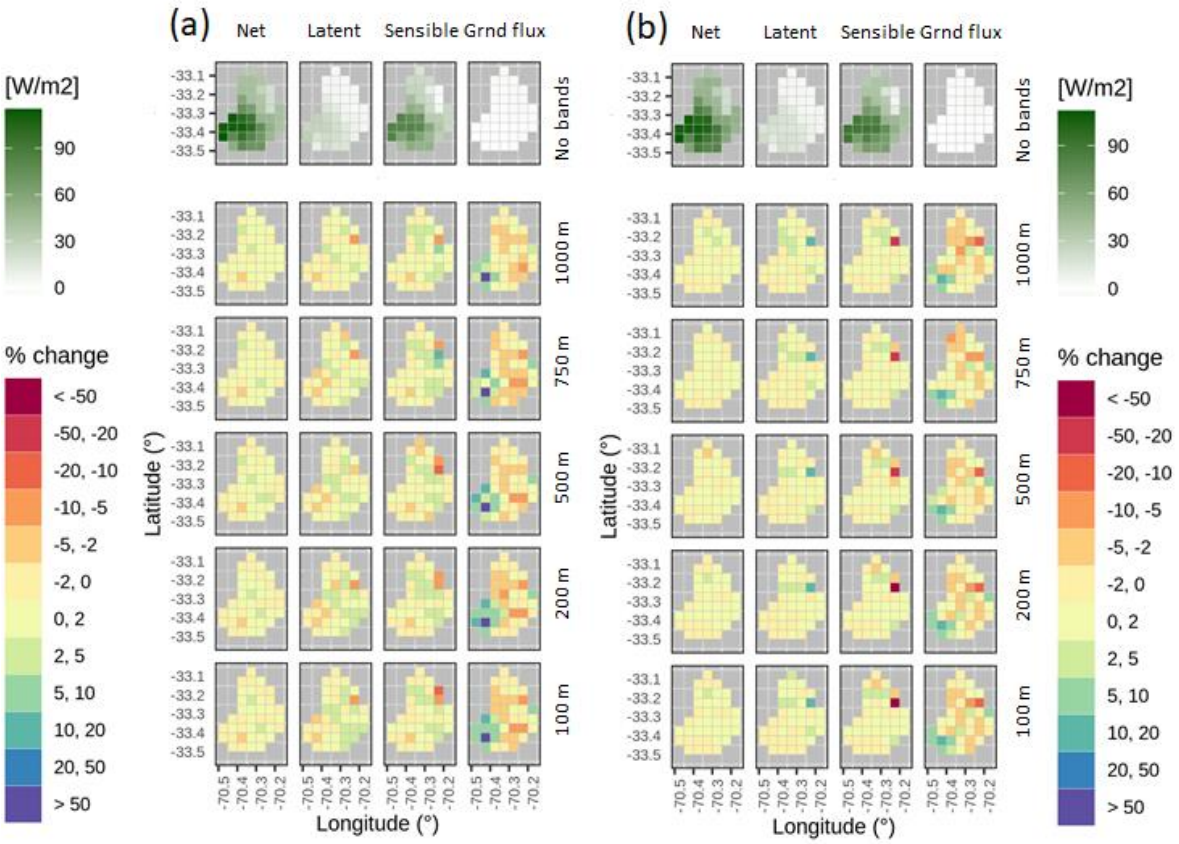

Figure S15: Spatial variability of percent changes [100*(alternative – benchmark)/benchmark] in grid cell-scale simulated mean annual energy fluxes at the Mapocho en Los Almendros basin. Results are presented for (a) wet and (b) dry analysis periods. The various columns display, from left to right, net radiation at the surface (including long and shortwave radiation), latent and sensible heat fluxes from the surface and ground heat flux plus heat storage in the top soil layer. The top row displays results for the benchmark model in W/m^2, while the remaining rows show results for alternative model configurations (i.e., 1000, 750, 500, 200 and 100 m elevation bands, from top to bottom). Black tiles indicate no data, associated to benchmark model results equal to zero (or unbounded result).

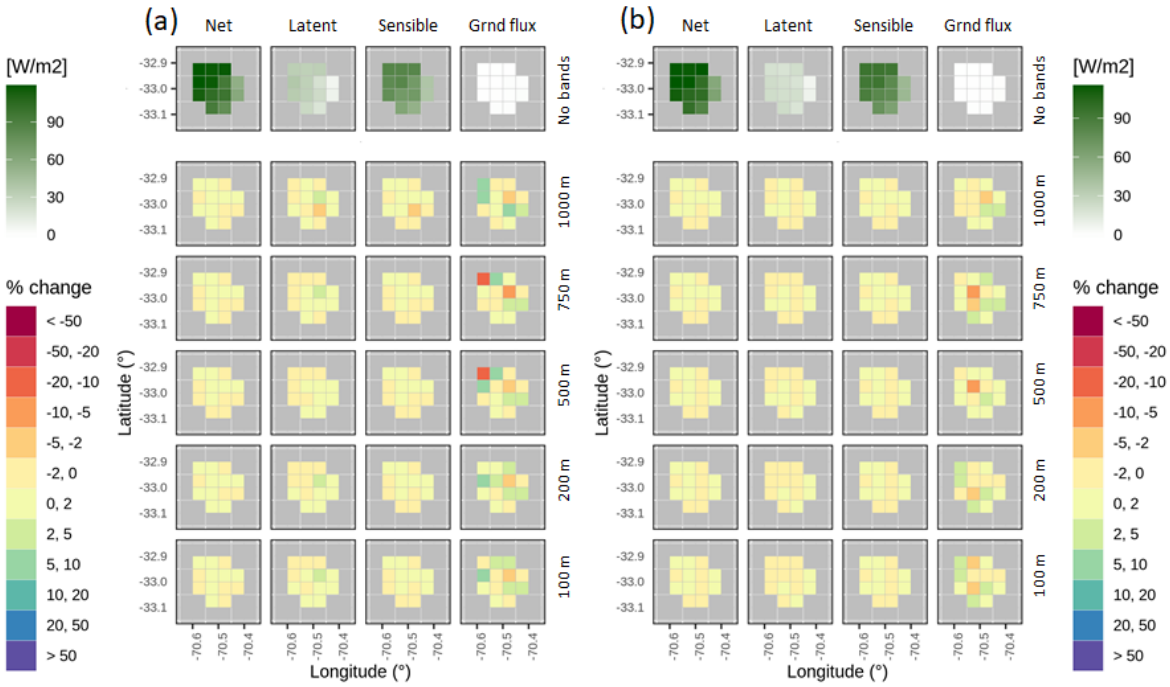

Figure S16: Same as in Figure S15, but for Pocuro en El Sifón.

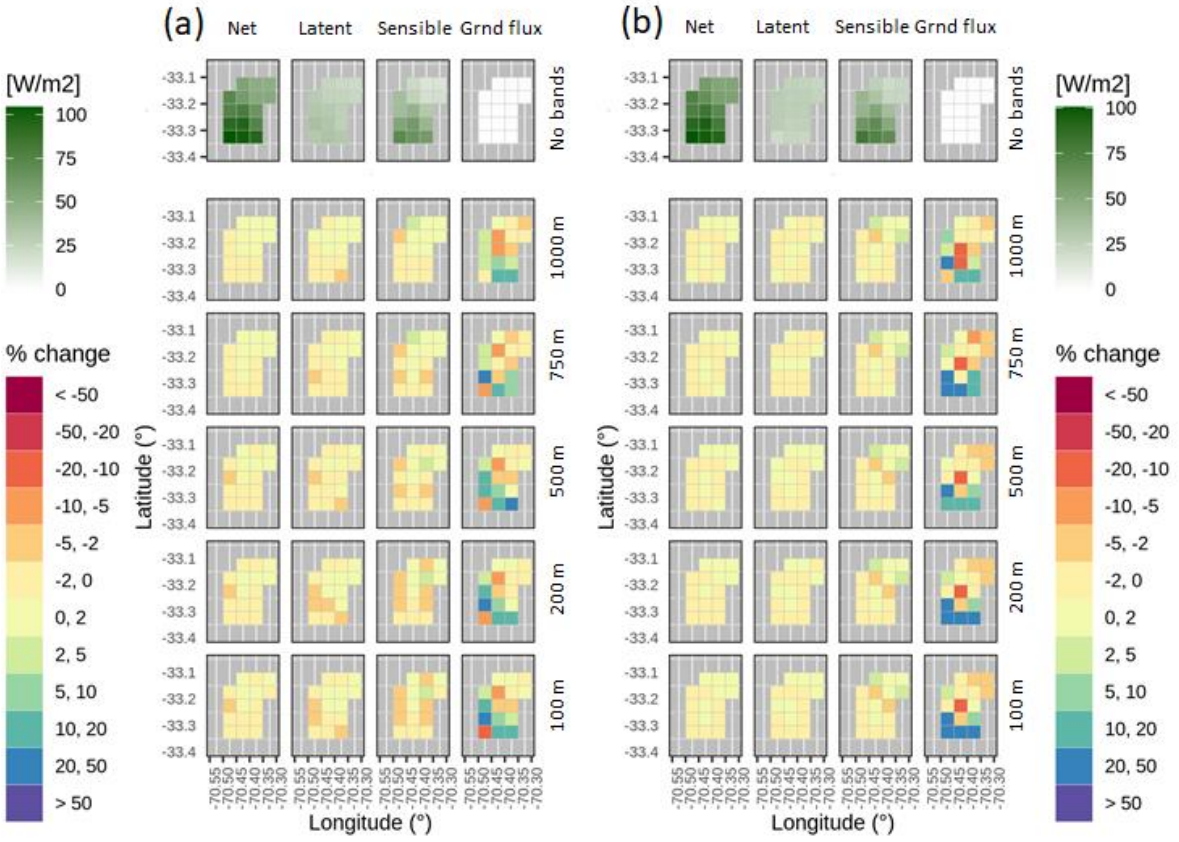

Figure S17: Same as in Figure S15, but for Arrayán en La Montosa.

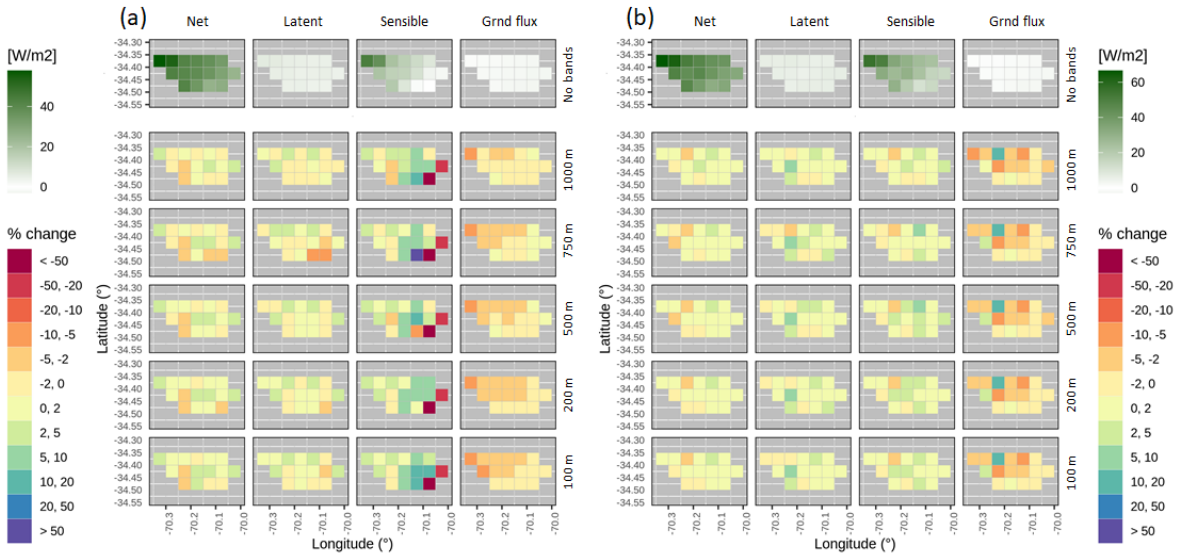

Figure S18: Same as in Figure S15, but for Las Leñas antes junta Río Cachapoal.

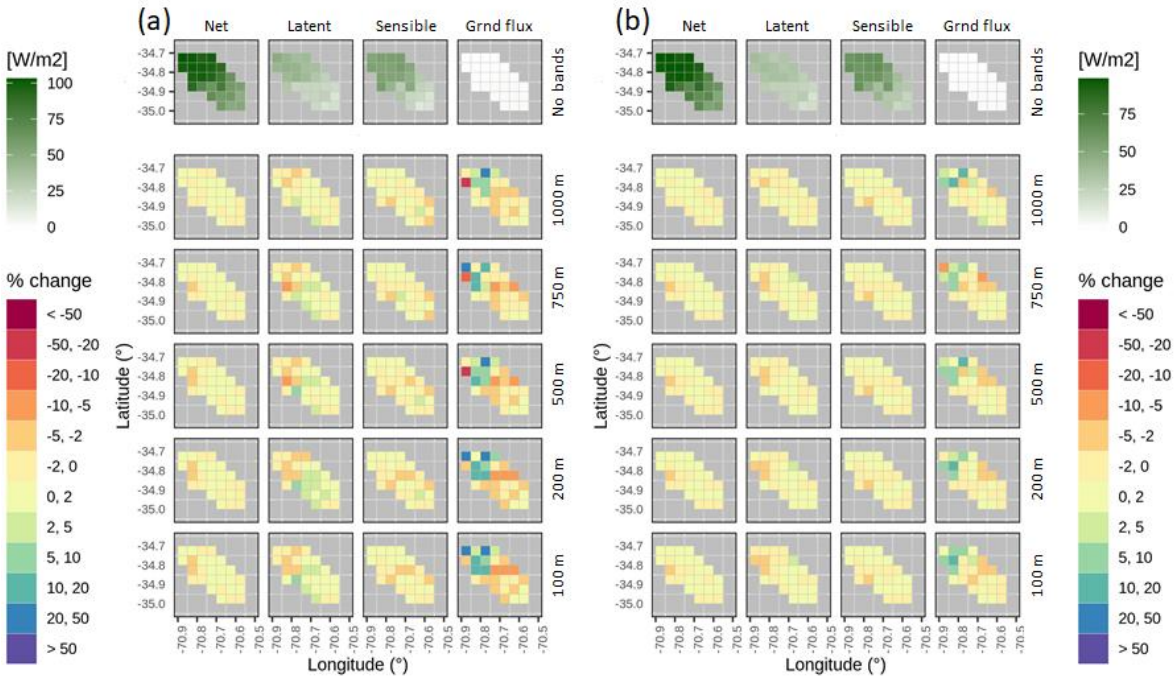

Figure S19: Same as in Figure S15, but for Río Claro en El Valle.

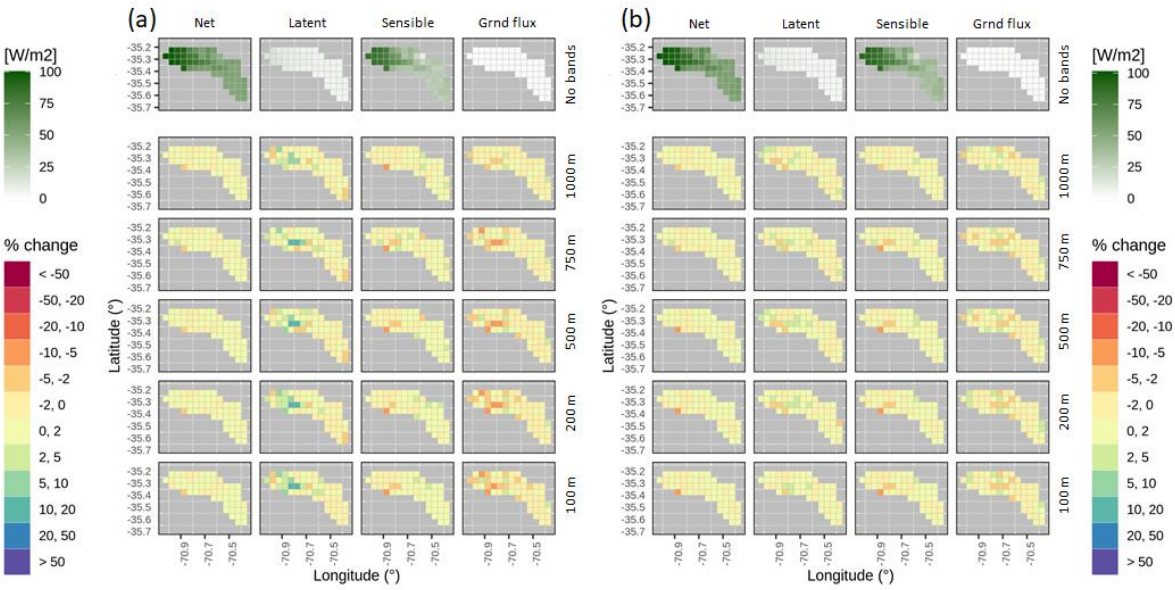

Figure S20: Same as in Figure S15, but for Río Colorado en junta con Palos.

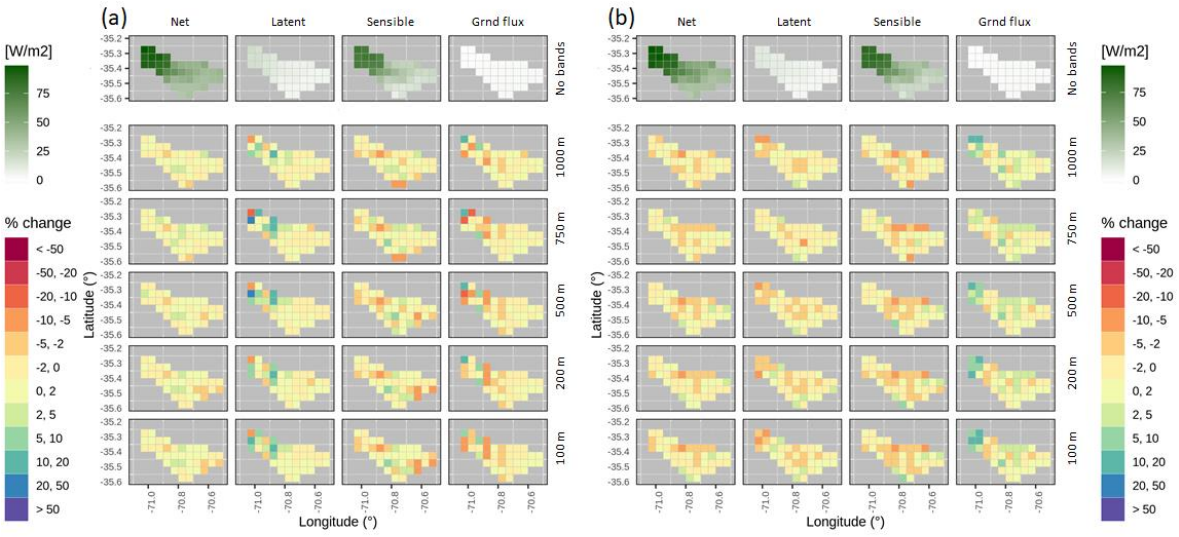

Figure S21: Same as in Figure S15, but for Río Palos en junta con Colorado.

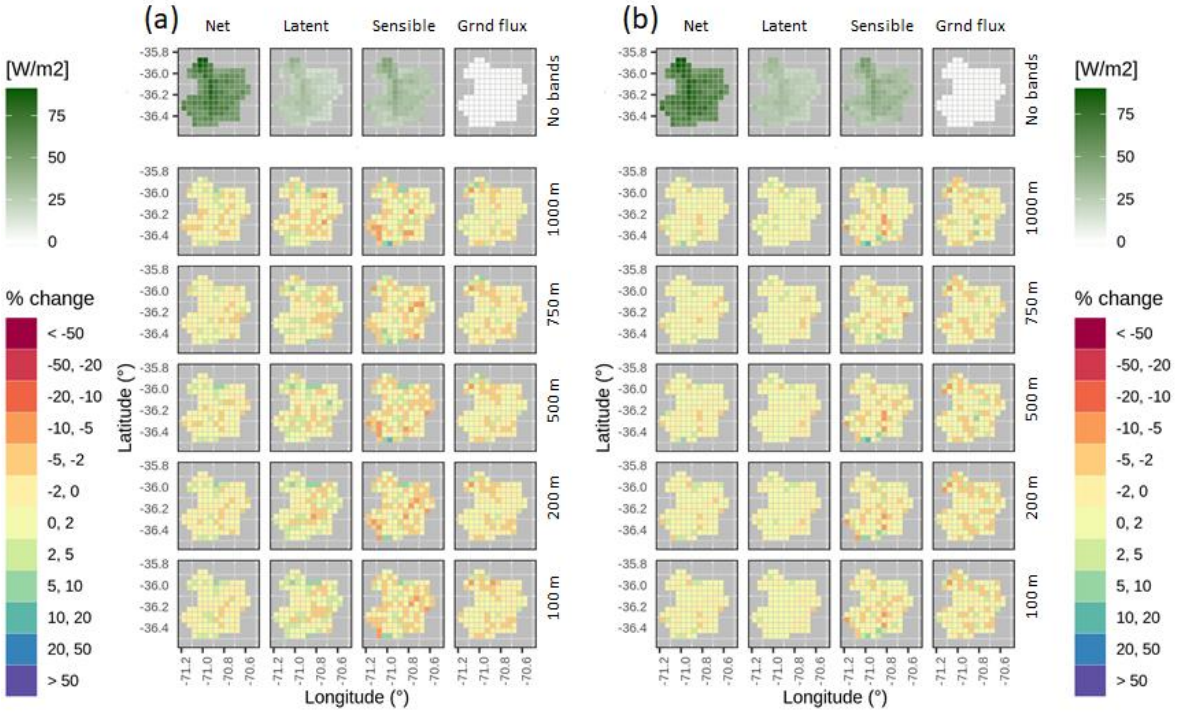

Figure S22: Same as in Figure S15, but for Río Melado en El Salto.

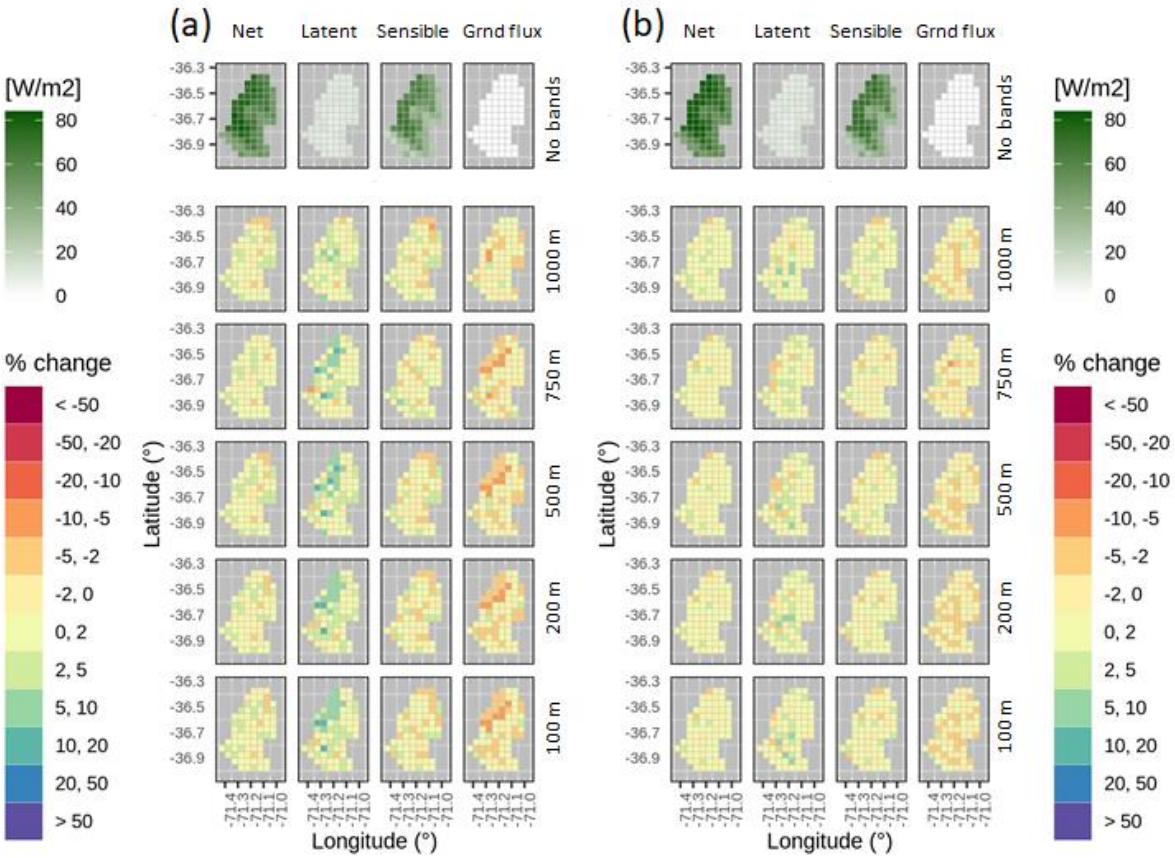

Figure S23: Same as in Figure S15, but for Río Ñuble en La Punilla.

III. CONCLUSIONES

En este trabajo de tesis, se han examinado y documentado las implicancias de representar la variabilidad espacial dentro de unidades de modelación a través de bandas de elevación en nueve cuencas andinas de Chile central. Para ello, se configuró el modelo hidrológico de macro-escala VIC y se calibró con una configuración sin bandas de elevación, y se realizaron simulaciones con cinco configuraciones de discretización vertical distintas, mediante bandas elevación cada 1000, 750, 500, 200 y 100 m. Los resultados se compararon con una simulación de referencia que no considera bandas de elevación, al igual que en las distintas etapas del proyecto de Actualización del Balance Hídrico Nacional (DGA, 2017, 2018, 2019a, 2019b). Se analizaron diferencias en términos de simulaciones de caudal, de flujos medios anuales y EAN del 1 de septiembre (utilizado para generar pronósticos estacionales de caudal en Chile central), además de simulaciones de EAN en un set de celdas ubicadas a lo largo de la cuenca del río Mapocho en los Almendros. Finalmente, se analizaron posibles características físico-climáticas que definen aquellas celdas donde, al agregar bandas de elevación, se produce un mayor impacto en las estimaciones de EAN.

Los resultados obtenidos en esta investigación muestran que, a pesar de que la incorporación de bandas de elevación no afecta de una forma apreciable el rendimiento del modelo en términos de la eficiencia de Kling-Gupta para caudales medios diarios y mensuales, sí se produce un efecto sobre otros flujos y el EAN a escala de cuenca, así como también en la variabilidad espacial de variables simuladas (al interior de la cuenca), sugiriendo un tipo de equifinalidad en la estructura del modelo. Otras conclusiones se listan a continuación:

- La inclusión de bandas de elevación produce el mayor efecto en la partición de la precipitación entre las fases líquida y sólida, tanto para la escala de cuenca como la escala de celda, con mayores variaciones durante el período húmedo analizado (Abril/1982 – Marzo/1987) en comparación al período seco (Abril/2010 – Marzo/2015). Además, las diferencias en evapotranspiración y escorrentía entre la simulación de referencia y las configuraciones alternativas (con bandas de elevación) son también más pronunciadas en el período húmedo, aunque no tan evidentes como para el caso de las fases líquida y sólida de la precipitación. Además, los impactos de la discretización vertical sobre el EAN del primero de septiembre son comparativamente más relevantes durante los períodos secos.
- La inclusión de bandas de elevación generalmente conlleva un menor derretimiento anual a la escala de cuenca, y más (menos) sublimación en cuencas limitadas por agua (limitadas por energía).
- La magnitud de las variaciones inducidas por las bandas de elevación en variables hidrológicas simuladas no es proporcional a la discretización vertical o al número de bandas de elevación adoptadas.
- Añadir más bandas de elevación afecta la duración de la cobertura de nieve, puesto que las bandas de elevación más altas mantienen nieve por un periodo de tiempo más prolongado. Además, se produce acumulación de nieve más temprano en el año hidrológico, en comparación con el modelo de referencia.

- El EAN del 1 de septiembre es generalmente más afectado por las bandas de elevación en celdas con menor altitud media, cuyo rango de elevación es mayor a 1000 m, con una pendiente pronunciada (mayor a 15°) y precipitaciones anuales menores a 1000 mm que ocurren en un intervalo de pocos meses.

A partir de los resultados presentados en esta tesis, se desprende que:

i. Si el objetivo de una simulación es mejorar la representación de los procesos de acumulación y derretimiento de la nieve, se debiera incluir bandas de elevación en al menos aquellas celdas que son más sensibles a la variabilidad vertical (e.g., unidades hidrológicas con altitud promedio baja pero que abarquen rango amplio de elevaciones). No obstante, El aumento de la discretización vertical conlleva un incremento en los tiempos de cómputo, por lo que se aconseja priorizar la discretización vertical en sectores (o URH's) sensibles, y no extenderla en el dominio completo.
ii. Debido a que una mayor cantidad de bandas de elevación no genera un impacto proporcional en los flujos y variables de estado simulados, y considerando que no hubo mayores diferencias con respecto a la configuración de 100 m, se considera que una resolución vertical de 200 m es lo suficientemente fina para representar los principales procesos por los cuales atraviesa el manto nival.

Investigaciones futuras podrían expandir los análisis para considerar la influencia de la orografía en la precipitación, flujos radiativos incidentes u otras forzantes meteorológicas, además de analizar las implicancias en el balance energético. También se recomienda probar con discretizaciones verticales irregulares al delinear bandas de elevación, dando énfasis (i.e., mayor resolución) a la representación de las áreas con mayor EAN. Adicionalmente sería de utilidad evaluar el efecto que las diferentes configuraciones de bandas de elevación tienen en pronósticos de caudal o proyecciones de impacto del cambio climático sobre distintas variables hidrológicas.

BIBLIOGRAFÍA

Abbaspour, K. C., Yang, J., Maximov, I., Siber, R., Bogner, K., Mieleitner, J., et al. (2007). Modelling hydrology and water quality in the pre-alpine/alpine Thur watershed using SWAT. *Journal of Hydrology*, *333*(2–4), 413–430. https://doi.org/10.1016/j.jhydrol.2006.09.014

Abdulla, F. A., Lettenmaier, D. P., Wood, E. F., & Smith, J. A. (1996). Application of a macroscale hydrologic model to estimate the water balance of the Arkansas-Red River Basin. *Journal of Geophysical Research: Atmospheres*, *101*(D3), 7449–7459. https://doi.org/10.1029/95JD02416

Addor, N., & Melsen, L. A. (2019). Legacy, Rather Than Adequacy, Drives the Selection of Hydrological Models. *Water Resources Research*, *55*(1), 378–390. https://doi.org/10.1029/2018WR022958

Aguayo, R., León-Muñoz, J., Garreaud, R., & Montecinos, A. (2021). Hydrological droughts in the southern Andes (40–45°S) from an ensemble experiment using CMIP5 and CMIP6 models. *Scientific Reports*, *11*(1), 1–16. https://doi.org/10.1038/s41598-021-84807-4

Alvarez-Garreton, C., Mendoza, P. A., Pablo Boisier, J., Addor, N., Galleguillos, M., Zambrano-Bigiarini, M., et al. (2018). The CAMELS-CL dataset: Catchment attributes and meteorology for large sample studies-Chile dataset. *Hydrology and Earth System Sciences*, *22*(11), 5817–5846. https://doi.org/10.5194/hess-22-5817-2018

Andreadis, K. M., & Lettenmaier, D. P. (2006). Assimilating remotely sensed snow observations into a macroscale hydrology model. *Advances in Water Resources*, *29*(6), 872–886. https://doi.org/10.1016/j.advwatres.2005.08.004

Andreadis, K. M., Storck, P., & Lettenmaier, D. P. (2009). Modeling snow accumulation and ablation processes in forested environments. *Water Resources Research*, *45*, W05429. https://doi.org/10.1029/2008WR007042

Arola, A., & Lettenmaier, D. P. (1996). Effects of Subgrid Spatial Heterogeneity on GCM-Scale Land Surface Energy and Moisture Fluxes. *Journal of Climate*, *9*(6), 1339–1349. https://doi.org/10.1175/1520-0442(1996)009<1339:EOSSHO>2.0.CO;2

Arora, M., Singh, P., Goel, N. K., & Singh, R. D. (2008). Climate variability influences on hydrological responses of a large himalayan basin. *Water Resources Management*, *22*(10), 1461–1475. https://doi.org/10.1007/s11269-007-9237-1

Bajracharya, A. R., Bajracharya, S. R., Shrestha, A. B., & Maharjan, S. B. (2018). Climate change impact assessment on the hydrological regime of the Kaligandaki Basin, Nepal. *Science of the Total Environment*, *625*, 837–848. https://doi.org/10.1016/j.scitotenv.2017.12.332

Bandaragoda, C., Tarboton, D. G., & Woods, R. A. (2004). Application of TOPNET in the distributed model intercomparison project. *Journal of Hydrology*, *298*(1–4), 178–201. https://doi.org/10.1016/j.jhydrol.2004.03.038

Barnett, T. P., Adam, J. C., & Lettenmaier, D. P. (2005). Potential impacts of a warming climate on water availability in snow-dominated regions. *Nature*, *438*(7066), 303–9. https://doi.org/10.1038/nature04141

Beck, H. E., Pan, M., Lin, P., Seibert, J., van Dijk, A. I. J. M., & Wood, E. F. (2020). Global Fully Distributed Parameter Regionalization Based on Observed Streamflow From 4,229 Headwater Catchments. *Journal of Geophysical Research: Atmospheres*, *125*(17).

https://doi.org/10.1029/2019JD031485
Bhatta, B., Shrestha, S., Shrestha, P. K., & Talchabhadel, R. (2019). Evaluation and application of a SWAT model to assess the climate change impact on the hydrology of the Himalayan River Basin. *Catena*, *181*(June), 104082. https://doi.org/10.1016/j.catena.2019.104082
Bras, R. (1990). *Hydrology: An Introduction to Hydrologic Sciences*. (Addison-Wesley, Ed.).
C3S, & Copernicus Climate Change Service (C3S). (2017). ERA5: Fifth generation of ECMWF atmospheric reanalyses of the global climate. Retrieved January 20, 2018, from https://cds.climate.copernicus.eu/cdsapp#!/home
Cherkauer, K. A., & Lettenmaier, D. P. (2003). Simulation of spatial variability in snow and frozen soil. *Journal of Geophysical Research*, *108*(D22), 8858. https://doi.org/10.1029/2003JD003575
Clark, M. P., Hendrikx, J., Slater, A. G., Kavetski, D., Anderson, B., Cullen, N. J., et al. (2011). Representing spatial variability of snow water equivalent in hydrologic and land-surface models: A review. *Water Resources Research*, *47*, W07539. https://doi.org/10.1029/2011WR010745
Clark, M. P., Nijssen, B., & Luce, C. H. (2017). An analytical test case for snow models. *Water Resources Research*, *53*(1), 909–922. https://doi.org/10.1002/2016WR019672
Clark, M. P., Vogel, R. M., Lamontagne, J. R., Mizukami, N., Knoben, W. J. M., Tang, G., et al. (2021). The Abuse of Popular Performance Metrics in Hydrologic Modeling. *Water Resources Research*, *57*(9), 1–16. https://doi.org/10.1029/2020WR029001
Deardorff, J. W. (1978). Efficient prediction of ground surface temperature and moisture, with inclusion of a layer of vegetation. *Journal of Geophysical Research*, *83*(C4), 1889. https://doi.org/10.1029/jc083ic04p01889
DeBeer, C. M., & Pomeroy, J. W. (2017). Influence of snowpack and melt energy heterogeneity on snow cover depletion and snowmelt runoff simulation in a cold mountain environment. *Journal of Hydrology*, *553*, 199–213. https://doi.org/10.1016/j.jhydrol.2017.07.051
Dee, D. P., Uppala, S. M., Simmons, A. J., Berrisford, P., Poli, P., Kobayashi, S., et al. (2011). The ERA-Interim reanalysis: Configuration and performance of the data assimilation system. *Quarterly Journal of the Royal Meteorological Society*, *137*(656), 553–597. https://doi.org/10.1002/qj.828
Demaria, E. M. C., Roundy, J. K., Wi, S., & Palmer, R. N. (2016). The effects of climate change on seasonal snowpack and the hydrology of the Northeastern and Upper Midwest United States. *Journal of Climate*, *29*(18), 6527–6541. https://doi.org/10.1175/JCLI-D-15-0632.1
DGA. (2017). *Actualización del balance hídrico nacional, SIT N°417, Ministerio de Obras Públicas, Dirección General de Aguas, División de Estudios y Planificación*. Santiago, Chile.
DGA. (2018). Aplicación de la metodología de actualización del balance hídrico nacional en las cuencas de las macrozonas norte y centro. SIT N° 435. Realizado por Universidad de Chile y Pontificia Universidad Católica. *Gobierno de Chile Ministerio de Obras Públicas*, 44.
DGA. (2019a). *Aplicación de la metodología de actualización del balance hídrico nacional en la macrozona sur y parte norte de la macrozona Austral, SIT N° 441.*
DGA. (2019b). Aplicación De La Metodología De Actualización Del Balance Hídrico Nacional En La Macrozona Sur Y Parte Norte De La Macrozona Austral. SIT N°441,

Ministerio de Obras Públicas, Dirección General de Aguas, Santiago, Chile. *Elaborado Por: Universidad de Chile, Facultad de Ciencias Físicas y Matemáticas.*

Didan, K. (2015). *MOD13Q1 MODIS/Terra Vegetation Indices 16-Day L3 Global 250m SIN Grid V006 [Data set]*. NASA EOSDIS Land Processes DAAC. Accessed from https://doi.org/10.5067/MODIS/MOD13Q1.006

Duan, Q. Y., Gupta, V. K., & Sorooshian, S. (1993). Shuffled complex evolution approach for effective and efficient global minimization. *Journal of Optimization Theory and Applications*, *76*(3), 501–521. https://doi.org/10.1007/BF00939380

Essery, R. (2003). Aggregated and distributed modelling of snow cover for a high-latitude basin. *Global and Planetary Change*, *38*(1–2), 115–120. https://doi.org/10.1016/S0921-8181(03)00013-4

Fontaine, T. A., Cruickshank, T. S., Arnold, J. G., & Hotchkiss, R. H. (2002). Development of a snowfall-snowmelt routine for mountainous terrain for the soil water assessment tool (SWAT). *Journal of Hydrology*, *262*(1–4), 209–223. https://doi.org/10.1016/S0022-1694(02)00029-X

Garreaud, R., Alvarez-Garreton, C., Barichivich, J., Pablo Boisier, J., Christie, D., Galleguillos, M., et al. (2017). The 2010-2015 megadrought in central Chile: Impacts on regional hydroclimate and vegetation. *Hydrology and Earth System Sciences*, *21*(12), 6307–6327. https://doi.org/10.5194/hess-21-6307-2017

Garreaud, R., Boisier, J. P. P., Rondanelli, R., Montecinos, A., Sepúlveda, H. H. H., & Veloso-Aguila, D. (2019). The Central Chile Mega Drought (2010–2018): A climate dynamics perspective. *International Journal of Climatology*, *40*(June), 1–19. https://doi.org/10.1002/joc.6219

Gericke, O. J., & Smithers, J. C. (2014). Revue des méthodes d'évaluation du temps de réponse d'un bassin versant pour l'estimation du débit de pointe. *Hydrological Sciences Journal*, *59*(11), 1935–1971. https://doi.org/10.1080/02626667.2013.866712

Grusson, Y., Sun, X., Gascoin, S., Sauvage, S., Raghavan, S., Anctil, F., & Sáchez-Pérez, J. M. (2015). Assessing the capability of the SWAT model to simulate snow, snow melt and streamflow dynamics over an alpine watershed. *Journal of Hydrology*, *531*, 574–588. https://doi.org/10.1016/j.jhydrol.2015.10.070

Gupta, H. V., Kling, H., Yilmaz, K. K., & Martinez, G. F. (2009). Decomposition of the mean squared error and NSE performance criteria: Implications for improving hydrological modelling. *Journal of Hydrology*, *377*(1–2), 80–91. https://doi.org/10.1016/j.jhydrol.2009.08.003

Habets, F., Etchevers, P., Golaz, C., Leblois, E., Ledoux, E., Martin, E., et al. (1999). Simulation of the water budget and the river flows of the Rhone basin. *Journal of Geophysical Research: Atmospheres*, *104*(D24), 31145–31172. https://doi.org/10.1029/1999JD901008

Haddeland, I., Matheussen, B. V., & Lettenmaier, D. P. (2002). Influence of spatial resolution on simulated streamflow in a macroscale hydrologic model. *Water Resources Research*, *38*(7), 29-1-29–10. https://doi.org/10.1029/2001WR000854

Hartman, M. D., Baron, J. S., Lammers, R. B., Cline, D. W., Band, L. E., Liston, G. E., & Tague, C. (1999). Simulations of snow distribution and hydrology in a mountain basin. *Water Resources Research*, *35*(5), 1587–1603. https://doi.org/10.1029/1998WR900096

Helfricht, K., Schöber, J., Seiser, B., Fischer, A., Stötter, J., & Kuhn, M. (2012). Snow accumulation of a high alpine catchment derived from LiDAR measurements. *Advances in Geosciences*, *32*, 31–39. https://doi.org/10.5194/adgeo-32-31-2012

IPCC. (2021). Assessment Report 6 Climate Change 2021: The Physical Science Basis.

Khatami, S., Peel, M. C., Peterson, T. J., & Western, A. W. (2019). Equifinality and Flux Mapping: A New Approach to Model Evaluation and Process Representation Under Uncertainty. *Water Resources Research*, *55*(11), 8922–8941. https://doi.org/10.1029/2018WR023750

Knoben, W. J. M., Woods, R. A., & Freer, J. E. (2018). A Quantitative Hydrological Climate Classification Evaluated With Independent Streamflow Data. *Water Resources Research*, *54*(7), 5088–5109. https://doi.org/10.1029/2018WR022913

Lehning, M., Völksch, I., Gustafsson, D., Nguyen, T. A., Stähli, M., & Zappa, M. (2006). ALPINE3D: a detailed model of mountain surface processes and its application to snow hydrology. *Hydrological Processes*, *20*(10), 2111–2128. https://doi.org/10.1002/hyp.6204

Li, D., Wrzesien, M. L., Durand, M., Adam, J., & Lettenmaier, D. P. (2017). How much runoff originates as snow in the western United States, and how will that change in the future? *Geophysical Research Letters*. https://doi.org/10.1002/2017GL073551

Liang, X., Lettenmaier, D. P., Wood, E. F., & Burges, S. J. (1994). A simple hydrologically based model of land surface water and energy fluxes for general circulation models. *Journal of Geophysical Research*, *99*(D7), 14,415.14.428. https://doi.org/10.1029/94jd00483

Liang, X., Wood, E. F., & Lettenmaier, D. P. (1996). Surface soil moisture parameterization of the VIC-2L model: Evaluation and modification. *Global and Planetary Change*, *13*(1–4), 195–206. https://doi.org/10.1016/0921-8181(95)00046-1

Liston, G., & Sturm, M. (1998). A snow-transport model for complex terrain. *Journal of Glaciology*.

López-Moreno, J. I., Pomeroy, J. W., Revuelto, J., & Vicente-Serrano, S. M. (2013). Response of snow processes to climate change: spatial variability in a small basin in the Spanish Pyrenees. *Hydrological Processes*, *27*(18), 2637–2650. https://doi.org/10.1002/hyp.9408

Markstrom, S. L., Niswonger, R. G., Regan, R. S., Prudic, D. E., & Barlow, P. M. (2008). *GSFLOW — Coupled Ground-Water and Surface-Water Flow Model Based on the Integration of the Precipitation-Runoff Modeling System (PRMS) and the Modular Ground-Water Flow Model (MODFLOW-2005). Methods*.

Masiokas, M. H., Rabatel, A., Rivera, A., Ruiz, L., Pitte, P., Ceballos, J. L., et al. (2020). A Review of the Current State and Recent Changes of the Andean Cryosphere. *Frontiers in Earth Science*, *8*(June), 1–27. https://doi.org/10.3389/feart.2020.00099

Melsen, L. A., Teuling, A. J., Torfs, P. J. J. F., Zappa, M., Mizukami, N., Mendoza, P. A., et al. (2019). Subjective modeling decisions can significantly impact the simulation of flood and drought events. *Journal of Hydrology*, *568*(November 2018), 1093–1104. https://doi.org/10.1016/j.jhydrol.2018.11.046

Mendoza, P. A., Rajagopalan, B., Clark, M. P., Cortés, G., & McPhee, J. (2014). A robust multimodel framework for ensemble seasonal hydroclimatic forecasts. *Water Resources Research*, *50*(7), 6030–6052. https://doi.org/10.1002/2014WR015426

Mendoza, P. A., Clark, M. P., Mizukami, N., Gutmann, E. D., Arnold, J. R., Brekke, L. D., & Rajagopalan, B. (2016). How do hydrologic modeling decisions affect the portrayal of climate change impacts? *Hydrological Processes*, *30*(7), 1071–1095. https://doi.org/10.1002/hyp.10684

Mendoza, P. A., Shaw, T. E., McPhee, J., Musselman, K. N., Revuelto, J., & MacDonell, S.

(2020). Spatial Distribution and Scaling Properties of Lidar-Derived Snow Depth in the Extratropical Andes. *Water Resources Research*, *56*(12). https://doi.org/10.1029/2020WR028480

Mizukami, N., P. Clark, M., G. Slater, A., D. Brekke, L., M. Elsner, M., R. Arnold, J., et al. (2014). Hydrologic Implications of Different Large-Scale Meteorological Model Forcing Datasets in Mountainous Regions. *Journal of Hydrometeorology*, *15*(1), 474–488. https://doi.org/10.1175/JHM-D-13-036.1

Mizukami, N., Clark, M. P., Gutmann, E. D., Mendoza, P. A., Newman, A. J., Nijssen, B., et al. (2016). Implications of the Methodological Choices for Hydrologic Portrayals of Climate Change over the Contiguous United States: Statistically Downscaled Forcing Data and Hydrologic Models. *Journal of Hydrometeorology*, *17*(1), 73–98. https://doi.org/10.1175/JHM-D-14-0187.1

Myneni, R., Knyazikhin, Y., Park, T. (2015). *MCD15A2H MODIS/Terra+Aqua Leaf Area Index/FPAR 8-day L4 Global 500m SIN Grid V006 [Data set]*. NASA EOSDIS Land Processes DAAC. Accessed from https://doi.org/10.5067/MODIS/MCD15A2H.006

NASA/METI/AIST/Japan Spacesystems and U.S./Japan ASTER Science Team (2001). *ASTER DEM Product* [Version 3]. NASA EOSDIS Land Processes DAAC. Accessed 2021-05-16 from https://doi.org/10.5067/ASTER/AST14DEM.003

Nash, J., & Sutcliffe, J. (1970). River flow forecasting through conceptual models part I - A discussion of principles. *Journal of Hydrology*, *10*(3), 282–290. https://doi.org/10.1016/0022-1694(70)90255-6

Newman, A. J., Clark, M. P., Winstral, A., Marks, D., & Seyfried, M. (2014). The Use of Similarity Concepts to Represent Sub-grid Variability in Land-Surface Models: Case Study in a Snowmelt Dominated Watershed. *Journal of Hydrometeorology*, In Press. https://doi.org/10.1175/JHM-D-13-038.1

Newman, A. J., Mizukami, N., Clark, M. P., Wood, A. W., Nijssen, B., & Nearing, G. (2017). Benchmarking of a physically based hydrologic model. *Journal of Hydrometeorology*, *18*(8), 2215–2225. https://doi.org/10.1175/JHM-D-16-0284.1

Pradhanang, S. M., Anandhi, A., Mukundan, R., Zion, M. S., Pierson, D. C., Schneiderman, E. M., et al. (2011). Application of SWAT model to assess snowpack development and streamflow in the Cannonsville watershed, New York, USA. *Hydrological Processes*, *25*(21), 3268–3277. https://doi.org/10.1002/hyp.8171

Prata, A. J. (1996). A new long-wave formula for estimating downward clear-sky radiation at the surface. *Quarterly Journal of the Royal Meteorological Society*, *122*(533), 1127–1151. https://doi.org/10.1002/qj.49712253306

Quintana, J., & Aceituno, P. (2012). Changes in the rainfall regime along the extratropical west coast of South America (Chile): 30-43º S. *Atmósfera*, *25*(1), 1–22.

Ragettli, S., Cortés, G., McPhee, J., & Pellicciotti, F. (2014). An evaluation of approaches for modelling hydrological processes in high-elevation, glacierized Andean watersheds. *Hydrological Processes*, *28*(23), 5674–5695. https://doi.org/10.1002/hyp.10055

Raleigh, M. S., Lundquist, J. D., & Clark, M. P. (2015). Exploring the impact of forcing error characteristics on physically based snow simulations within a global sensitivity analysis framework. *Hydrology and Earth System Sciences*, *19*(7), 3153–3179. https://doi.org/10.5194/hess-19-3153-2015

Rasmussen, R., Ikeda, K., Liu, C., Gochis, D., Clark, M., Dai, A., et al. (2014). Climate Change Impacts on the Water Balance of the Colorado Headwaters: High-Resolution Regional Climate Model Simulations. *Journal of Hydrometeorology*, *15*(3), 1091–1116.

https://doi.org/10.1175/JHM-D-13-0118.1
Schneider, D., & Molotch, N. P. (2016). Real-time estimation of snow water equivalent in the Upper Colorado River Basin using MODIS-based SWE Reconstructions and SNOTEL data. *Water Resources Research*, *52*(10), 7892–7910. https://doi.org/10.1002/2016WR019067
Sepúlveda, U. M., Mendoza, P. A., Mizukami, N., & Newman, A. J. (2021). Revisiting parameter sensitivities in the Variable Infiltration Capacity model. *Hydrology and Earth System Sciences Discussions*, (November), in review. https://doi.org/https://doi.org/10.5194/hess-2021-550
Thornton, P. E., & Running, S. W. (1999). An improved algorithm for estimating incident daily solar radiation from measurements of temperature, humidity, and precipitation. *Agricultural and Forest Meteorology*, *93*(4), 211–228. https://doi.org/10.1016/S0168-1923(98)00126-9
Tong, J., Déry, S., & Jackson, P. (2008). Topographic control of snow distribution in an alpine watershed of western Canada inferred from spatially-filtered MODIS snow products. *Hydrology and Earth System Sciences Discussions*, *5*(4), 2347–2371. https://doi.org/10.5194/hessd-5-2347-2008
USACE. (1956). *Snow Hidrology. Summary Report of the Snow Investigations*. Oregon. https://doi.org/92069877
Vargas, X., Gómez, T., Ahumada, F., Rubio, E., Cartes, M., & Gibbs, M. (2013). Water availability in a mountainous Andean watershed under CMIP5 climate change scenarios. *IAHS-AISH Proceedings and Reports*, *360*(July), 33–38.
Vásquez, N., Cepeda, J., Gómez, T., Mendoza, P. A., Lagos, M., Boisier, J. P., et al. (2021). Catchment-Scale Natural Water Balance in Chile. In *Water Resources of Chile* (pp. 189–208). https://doi.org/10.1007/978-3-030-56901-3_9
Vicuña, S., Garreaud, R. D., & McPhee, J. (2011). Climate change impacts on the hydrology of a snowmelt driven basin in semiarid Chile. *Climatic Change*, *105*(3–4), 469–488. https://doi.org/10.1007/s10584-010-9888-4
Vicuña, S., Vargas, X., Boisier, J. P., Mendoza, P. A., Gómez, T., Vásquez, N., & Cepeda, J. (2021). Impacts of Climate Change on Water Resources in Chile. In *Water Resources of Chile* (Vol. 13, pp. 347–363). https://doi.org/10.1007/978-3-030-56901-3_19
Voordendag, A., Réveillet, M., MacDonell, S., & Lhermitte, S. (2021). Snow model comparison to simulate snow depth evolution and sublimation at point scale in the semi-arid Andes of Chile. *Cryosphere*, *15*(9), 4241–4259. https://doi.org/10.5194/tc-15-4241-2021
Yilmaz, K. K., Gupta, H. V., & Wagener, T. (2008). A process-based diagnostic approach to model evaluation: Application to the NWS distributed hydrologic model. *Water Resources Research*, *44*(9), W09417. https://doi.org/10.1029/2007WR006716
Zhao, Y., Feng, D., Yu, L., Wang, X., Chen, Y., Bai, Y., et al. (2016). Detailed dynamic land cover mapping of Chile: Accuracy improvement by integrating multi-temporal data. *Remote Sensing of Environment*, *183*, 170–185. https://doi.org/10.1016/j.rse.2016.05.016